Quaternary Research xxx (2013) xxx–xxx

Contents lists available at SciVerse ScienceDirect

Quaternary Research

journal homepage: www.elsevier.com/locate/yqres

Late Neanderthals at Jarama VI (central Iberia)?

Martin Kehl [a,*], Christoph Burow [a], Alexandra Hilgers [a], Marta Navazo [b,c], Andreas Pastoors [d], Gerd-Christian Weniger [d,e], Rachel Wood [f], Jesús F. Jordá Pardo [g]

[a] University of Cologne, Institute of Geography, Albertus-Magnus-Platz, 50923 Cologne, Germany
[b] Área de Prehistoria, Departamento de Ciencias Históricas y Geografía, Universidad de Burgos, Plaza Misael Bañuelos s/n, E-09001 Burgos, Spain
[c] Centro Nacional de Investigación sobre la Evolución Humana (CENIEH), Paseo Sierra de Atapuerca s/n, E-09002 Burgos, Spain
[d] Neanderthal Museum, Talstr. 300, 40822 Mettmann, Germany
[e] University of Cologne, Institute of Prehistoric Archaeology, Albertus-Magnus-Platz, 50923 Cologne, Germany
[f] Research School of Earth Sciences, The Australian National University, 1 Mills Road, Canberra, ACT 0200, Australia
[g] Laboratorio de Estudios Paleolíticos, Departamento de Prehistoria y Arqueología, Universidad Nacional de Educación a Distancia, Paseo Senda del Rey, 7. Ciudad Universitaria, E-28040 Madrid, Spain

ARTICLE INFO

Article history:
Received 30 January 2013
Available online xxxx

Keywords:
Slackwater deposits
Mineralogy
Geochemistry
Micromorphology
Luminescence dating
Radiocarbon dating
Middle Paleolithic
Stone industry

ABSTRACT

Previous geochronological and archaeological studies on the rock shelter Jarama VI suggested a late survival of Neanderthals in central Iberia and the presence of lithic assemblages of Early Upper Paleolithic affinity. New data on granulometry, mineralogical composition, geochemical fingerprints and micromorphology of the sequence corroborate the previous notion that the archaeological units JVI.2.1 to JVI.2.3 are slackwater deposits of superfloods, which did not experience significant post-depositional changes, whereas the artifact-rich units JVI.3 and JVI.1 mainly received sediment inputs by sheetwash and cave spall. New AMS radiocarbon measurements on three samples of cut-marked bone using the ultrafiltration technique yielded ages close to, or beyond, the limit of radiocarbon dating at ca. 50 ^{14}C ka BP, and hence suggest much higher antiquity than assumed previously. Furthermore, elevated temperature post-IR IRSL luminescence measurements on K feldspars yielded burial ages for subunits JVI.2.2 and JVI.2.3 between 50 and 60 ka. Finally, our reappraisal of the stone industry strongly suggests that the whole sequence is of Mousterian affinity. In conclusion, Jarama VI most probably does not document a late survival of Neanderthals nor an Early Upper Paleolithic occupation in central Iberia, but rather indicates an occupation breakdown after the Middle Paleolithic.

Introduction

Human occupation of the Iberian Peninsula during the late Pleistocene is concentrated on the coastal strip and its hinterland, whereas evidence for human presence in the interior is significantly lower (Bicho et al., 2007). This pattern is particularly evident in the Early Upper Paleolithic where the interior seems to be abandoned by humans (Delibes de Castro and Díez Martín, 2006; Cacho et al., 2010; Schmidt et al., 2012). In contrast, Neanderthals occupied central Iberia in the Late Middle Paleolithic as demonstrated by Mousterian assemblages and Neanderthal fossils from, for example, Cueva de la Ermita, Cueva Millán (Moure and García-Soto, 2000; Díez et al., 2008), Prado Vargas (Navazo and Diéz, 2008), Peña Capón, Valdegoba (Díez et al., 1988–89), and Jarama VI (Jordá Pardo, 2001).

Besides lithic assemblages of Middle Paleolithic character, the presence of Neanderthals was postulated based on an undiagnostic human fossil from Jarama VI (Lorenzo et al., 2012). The human metatarsal fragment was embedded in fluvial sands and silts forming the middle stratigraphic subunit of Jarama VI (JVI.2.2). This subunit contained scattered archaeological remains (bones and lithics), some concentrated around a small hearth. The underlying, archaeologically sterile subunit JVI.2.3 separates these finds from a rich Mousterian assemblage and bones of micro- and macro-mammals excavated from the gravelly deposit of unit JVI.3. Archaeological material was also found in lutitic sands of subunit JVI.2.1. The uppermost unit, unit JVI.1, contained artifacts that have been preliminarily attributed to the Upper Paleolithic (Jordá Pardo, 2001).

The chronological frameworks of this and other Middle Paleolithic sequences in central Iberia are still unreliable as few radiometric ages are available. At Jarama VI, three conventional radiocarbon measurements of charcoal, directly associated with human activity (Zilhão, 2006) gave age estimates of 29.4–26.9 cal ka BP (Beta 56640), 44.1–29.8 cal cal BP (Beta 56639) and 42.6–34.5 cal ka BP (Beta 56638) at 95.4% probability for the stratigraphic sequence of archaeological

* Corresponding author.
E-mail addresses: kehlm@uni-koeln.de (M. Kehl), mnavazo@ubu.es (M. Navazo), pastoors@neanderthal.de (A. Pastoors), weniger@neanderthal.de (G.-C. Weniger), rachel.wood@anu.edu.au (R. Wood), jjorda@geo.uned.es (J.F. Jordá Pardo).

0033-5894/$ – see front matter
http://dx.doi.org/10.1016/j.yqres.2013.06.010

units JVI.1, JVI2.1 (hearth feature) and JVI.2.2, respectively (Table 1). These radiocarbon dates suggest a late survival of Neanderthals in central Iberia, at a time when anatomically modern humans were already present in northern Iberia (Zilhão, 2006; Maroto et al., 2012).

The timing of Neanderthal disappearance in Iberia and a possible coexistence with modern humans are matters of dispute. A late survival of Neanderthals in southern Iberia has been inferred from young radiocarbon ages related to Mousterian layers at, for example, Gorham's cave, Gruta de Oliveira and Boquete de Zafarraya (Hublin et al., 1995; Finlayson et al., 2006; Zilhão, 2006) and was related to the presence of glacial refugia in the South (Finlayson and Carríon, 2007; Jennings et al., 2011). Schmidt et al. (2012) have demonstrated that AMS radiocarbon dates from Late Middle and Early Upper Paleolithic layers are scattered (cf. Higham et al., 2012). This scatter is most likely related to contamination or poor preservation of radiocarbon samples (Higham et al., 2009; Maroto et al., 2012; Wood et al., in press), but stratigraphic problems and difficulties in associating the sample with human activity have undoubtedly played a role in some cases (Zilhão, 2006). Therefore, it appears possible that the prolonged survival of Neanderthals in southern Iberia is not real but is related to problematic dates.

Jarama VI may play an important role for investigating a possible late survival of Neanderthals in central Iberia and the cultural transition towards the Upper Paleolithic. Based on new geoarchaeological research, we re-evaluated the geological and cultural sequences of Jarama VI. Here we provide detailed descriptions of the rock shelter deposits including new sedimentological, geochemical, mineralogical and micromorphological results and present a reappraisal of the lithic inventory. Finally, we present a revised chronological framework for Jarama VI based on new AMS radiocarbon and luminescence dates Table 2. These data shed new light on the hypotheses of a prolonged survival of Neanderthals in central Iberia.

Geographical setting and sediment sequence

The Upper Jarama Valley is located at the municipality of Valdesotos, on the northwestern edge of the Guadalajara province (Spain) (Fig. 1). This area is on the southern slope of the eastern part of the Central Range. It belongs to a region limited to the north by the Spanish Central Range (Somosierra and Sierra de Ayllón) and to the south by the tabular reliefs of the Madrid Tertiary Basin. In this area the Upper Jarama Valley cuts and runs through a narrow strip of dolomites, dolomitic limestones and limestones (Santonian, Upper Cretaceous) tilted towards the southwest (ITGE, 1990) and affected by a strong karstification. Discordant above the Cretaceous carbonate rocks appear detrital deposits of the Neogene made by alluvial fans generated in an early stage before the location and downcutting of the Jarama River during the Pleistocene. The karstic system is spanned by Jarama River, creating a karstic canyon with many caves and rock shelters in the cliffs of both banks, which are the proof of the different stages of the karstic development and the downcutting of the river. Some of these caves have Pleistocene and Holocene stratigraphic records (Jordá Pardo, 1993).

Table 2
Summary of lithic assemblages in the different archaeological levels of Jarama VI.

	JVI.1	JVI.2	JVI.3	Total
Hammer	47	179	178	404
Chopper	–	–	1	1
Cores	32	21	95	148
Retouched flakes	24	23	84	131
Flakes	220	119	810	1149
Total	323	343	1168	1833

The modern climate of the area is Meditarranean (Csb according to Koeppen, Atlas Climático Ibérico, sino ano) with a comparatively short dry season in the summer (Muñoz Muñoz et al., 1989). Mean annual temperature is around 12.5 °C, and mean annual precipitation amounts to ~700 to 900 mm, while both parameters change considerably with altitude in the mountainous area (Atlas Climático Ibérico, sino ano; Muñoz Muñoz et al., 1989). Little information is available on paleoclimatic conditions during marine oxygen isotope stage (MIS) 3, because terrestrial archives covering this period are scarce in central Iberia (cf. González-Sampériz et al., 2010; Moreno et al., 2012).

Sediment cores retrieved from the Villarquemado paleolake (40°30′N, 1°18′W, 987 m asl, Moreno et al., 2012) and the Fuentillejo maar (38°56′N, 4°3′W, 635 m asl, Vegas et al., 2010), located about 180 and 230 km to the ESE and SSW, respectively, of Jarama VI provide evidence for the occurrence of millennial-scale climatic changes in central Iberia. Based on lithological facies, magnetic susceptibility and geochemical proxies, sediment unit IV of the Villarquemado sequence accumulated in the distal part of an alluvial fan or in an ephemeral lake, reflecting dry climatic conditions during the lower half of MIS 3 (Moreno et al., 2012). After deposition of this most arid part of the whole sequence, sediment units III and II accumulated during the upper part of MIS 3. The sediment facies represent alterations of shallow carbonatic lake and clastic lake paleo-environments, the latter with fluvial influence, which were interpreted as reflecting millennial-scale fluctuations between moist and more arid climates. Lithological, geochemical, palynological (Vegas et al., 2010) and additional biomarker records (Ortiz et al., 2013) of the Fuentillejo core also reflect paleo-environmental changes with pulses of dry and cold climatic conditions, which were correlated with Heinrich events. Although age models for both sequences rely on few radiocarbon dates, only, and correlation with individual events of climate change is not very reliable, it appears to be very likely that millennial-scale climate change, well-documented in marine cores off Iberia (cf. Moreno et al., 2012 for further references), are also recorded in terrestrial archives of central Iberia.

The rock shelter Jarama VI is located about 23 m above the present water level of Jarama River, 822 m above sea level. Several remnants of fluvial terraces are preserved in the valley, the uppermost being located about 9 m below the opening of the shelter. Detailed descriptions

Table 1
Results of radiocarbon dates for the Paleolithic sequence at Jarama VI. Radiocarbon dates have been calibrated against IntCal09 (Reimer et al., 2009) in OxCal v.4 (Bronk Ramsey, 2009). To obtain a reliable date, collagen should comprise >1% of the dry bone weight, and have a $\delta^{13}C$ of ca. −20‰, C:N ratio of 2.9–3.4 and %C of ca. 44% (van Klinken, 1999) and charcoal should be rich in C (Rebollo et al., 2011).

Lab code	Unit	Square	Material	^{14}C-age	^{14}C std	cal BP (95.4% probability range)	Collagen yield (%)	$\delta^{13}C$	C:N	%C	Reference
Beta-56640	JVI.1	H-4	Charcoal	23,380	500	29,370–26,920	–	–	–	Low	Jordá Pardo, 2007
OxA 21714	JVI.1	D-3	Cut-marked pelvis fragment. Indeterminate species	>50,200	–	–	1.4	−19.3	3.4	46.9	Wood et al., in press
Beta-56638	JVI.2.1	D-4	Charcoal (hearth feature)	29,500	2700	44,090–29,830[a]				Low	Jordá Pardo, 2007
Beta-56639	JVI.2.2	F-4	charcoal	32,600	1860	42,580–34,450				Low	Jordá Pardo, 2007
OxA-X-2310-22	JVI.2.2	E-4	Cut-marked tibia/humerus. Indeterminate species	49,400	3 700		0.5	−18.2	3.2	43.2	Wood et al., in press
OxA-X-2290-56	JVI.3	D-4	Cut-marked diaphyseal fragment	>47,000			0.7	−18.8	3.3	45.3	Wood et al., in press

[a] Date may extend beyond the calibration curve.

Please cite this article as: Kehl, M., et al., Late Neanderthals at Jarama VI (central Iberia)?, Quaternary Research (2013), http://dx.doi.org/10.1016/j.yqres.2013.06.010

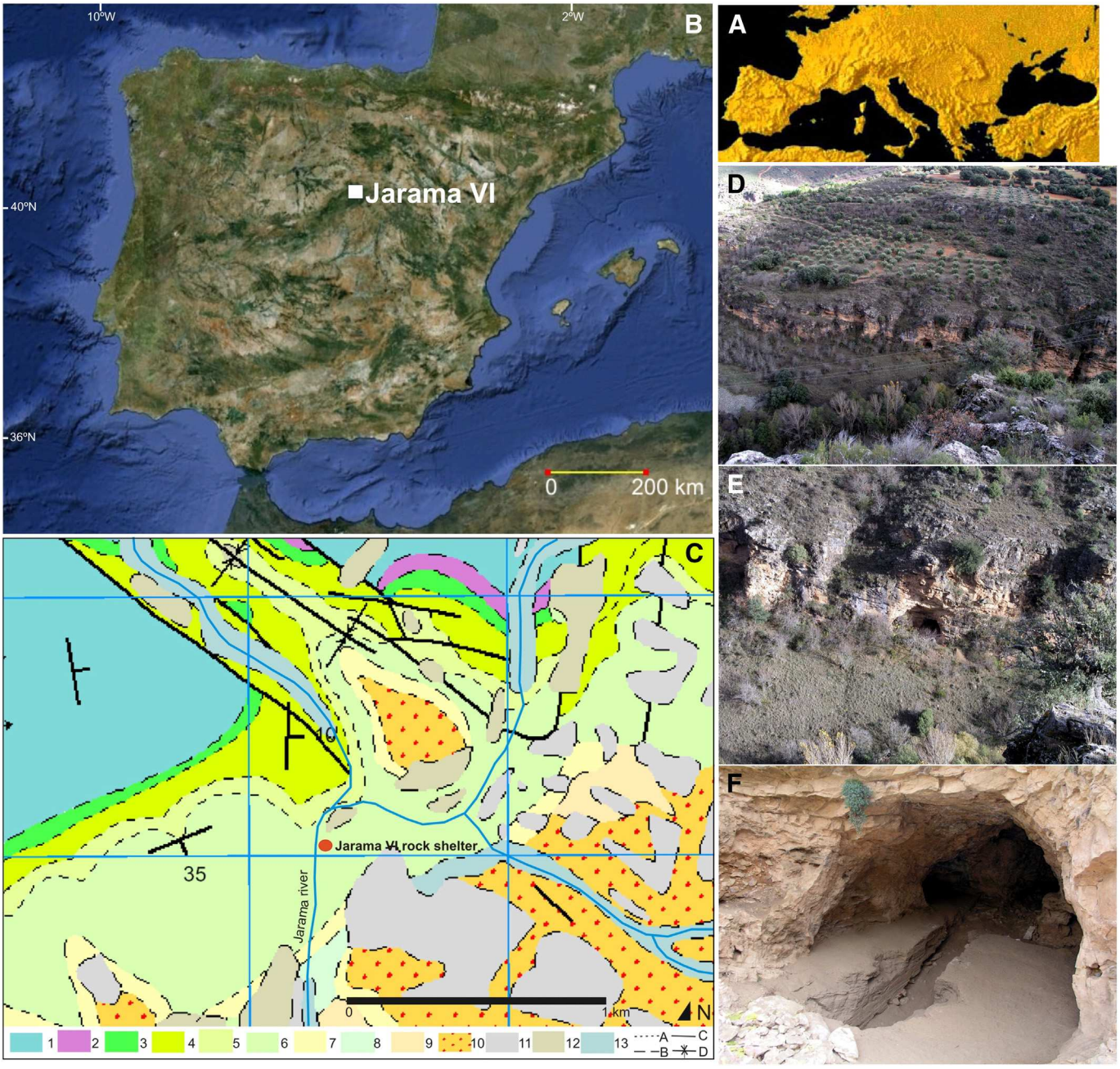

Figure 1. A, Location map of Jarama VI. B, Geological context of the Jarama VI rock shelter in the geologic map scale 1:50.000 (I.T.G.E., 1990). Legend: A: Concordant contact; B: Discordant contact; C: Fault; D: Sincline; Ordovician: 1, Black shales; Triassicc: 2, Sandstones and lutites; Upper Cretaceous: 3, Sands and lutites (Cenomanian), 4, Marls (Turonian), 5, Dolomites, limestones and marls (Coniacian), 6, Dolomites, dolomitic limestones and limestones (Santonian), 7, Marly dolomites and dolomitic marls (Campanian), 8, Dolomitic calcareous breccia (Campanian–Maastrichtian); Upper Cretaceous–Paleocene: 9, Red lutites, gypsum and conglomerates; Upper Miocene–Pliocene: 10, Conglomerates and lutites; Lower Pleistocene: 11, Pebbles, gravels, sands and clays; middle Pleistocene: 12, Pebbles, gravels, sands and clays; Holocene: 13, Alluvial deposits. B, C and D, Photos of the Jarama canyon and the Jarama VI rock shelter.

of the sedimentary fill of the shelter were presented by Jordá Pardo (2001, 2007) and are summarized briefly below.

The lowermost stratigraphic unit JVI.4 consists of carbonated white sands, 10–15 cm thick, which are a product of the dolomitic substratum weathering. The unit does not contain any archaeological materials or faunal remains. The overlying unit JVI.3, 5–60 cm thick, contains well-rounded shale gravels, shale and quartzite stones and abundant angular dolomitic boulders in a matrix of gray, brown and red-brown clayey sand (Fig. 2, North profile). The gravel and well-rounded boulders originate from the river, whereas angular and subangular dolomites were provided by roof fall probably linked to cryoclastic processes and later reworked by the river. The unit contains Mousterian lithic industry, as well as the bones of large herbivores (*Bos/Bison* sp., *Rupicapra rupicapra*, *Cervus elaphus*, *Equus caballus* and Rhinocerotidae indet.) and micromammals (*Microtus* sp., Rodentia indet.; Adán Alvarez et al., 1995).

Unit JVI.2, 10–160 cm thick, consists of laminated and homogeneous beds of silty sands and sands showing many features of fluvial deposition such as parallel or crossed lamination and stream ripples. The lower part of this unit (Unit JVI.2.3) is archaeologically sterile. In the north profile (Fig. 2), located near the cave entrance, it can be subdivided into four layers separated by erosional disconformities and paraconformities indicating at least four cycles of fluvial deposition and erosion. Interbedding with gray medium sands reflects

Please cite this article as: Kehl, M., et al., Late Neanderthals at Jarama VI (central Iberia)?, Quaternary Research (2013), http://dx.doi.org/10.1016/j.yqres.2013.06.010

deposition under high velocities of flow, but these layers readily disappear towards the interior, where unit JVI.2.3 thins (Fig. 2). The intermediate part (unit JVI.2.2) contained scattered archaeological finds, bone remains and a hearth feature. Farther inside the rock shelter, the uppermost unit JVI.2.1 contained numerous Mousterian lithic artifacts. The faunal remains are represented by large herbivores (*R. rupicapra*, *C. elaphus*), micromammals (*Pliomys* cf. *lenki*, *Microtus arvalis-agrestis* group, *Apodemus* sp., cf. *Oryctolagus cuniculus* and Rodentia indet), birds (*Alectoris rufa*, *Pica pica* and *Pyrrhocorax graculus*), amphibious (*Pelobates cultripes*) and Pisces indet. (Adán Alvarez et al., 1995). The sandy facies of unit JVI.2 are fluvial deposits with overflowing facies that, according to Jordá Pardo (2001, 2007), were deposited during a superflood.

Unit JVI.1 consists of reddish sands and clays with angular autochthonous dolomite fragments. Its lower limit is erosive. The dolomite derived from the cave ceiling by cryoclastic processes indicating a cold and dry environment and fine materials have been washed in. This unit contains a rich assemblage of lithic artifacts, previously attributed to the Early Upper Paleolithic (Jordá Pardo, 2001, 2007), as well as bone remains of large herbivores (*Bos/Bison* sp., *R. rupicapra*, *C. elaphus*, *E. caballus*, Rhinocerontidae indet. and Canidae indet.), micromammals (Soricidae indet., *M. arvalis-agrestis* group, *Allocricetus bursae*, *Sciurus vulgaris*, cf. *O. Cuniculus* and Rodentia indet.), birds (*A. Rufa*, *Coturnix coturnix*, *Columba livia/oenas*, *Bubo bubo*, *Falco* sp., *P. pica*, *Pyrrocorax*, *P. graculus*, *Corvus corone* and Corvidae indet.), reptiles (*Lacerta lepida*), and amphibious (*Bufo bufo*; Adán Alvarez et al., 1995). Furthermore, a *Homo* sp. tooth was recovered from sediments collapsed from unit JVI.1 between two consecutive excavation seasons.

In the interior of the cave, dolomite breccia and stalagmitic crust (unit 0) capped the stratigraphic sequence. The crust probably formed after a change towards warm and slightly moist climatic conditions.

Sedimentology, geochemistry, mineralogy and micromorphology

Sampling and methods

The North profile of Jarama VI and squares E to I of the West profile were described in the field and representative samples were taken from archaeological units JVI.2.2, and JVI.2.3 for granulometric and geochemical analyses. Two samples from unit JVI.1 were taken from the Northwest profile in squares F-5/E-5 and from the East profile in square J8. From the latter, a remnant of unit JVI.2.1 was sampled. Most of unit JVI.3 was omitted due to high contents of gravels and boulders. The sampling locations are indicated in Figure 2.

The sediment samples were dry-sieved. All determinations discussed below were conducted on the fine fraction (<2 mm in diameter). The granulometrical composition of the fine fraction (<2 mm in diameter) was determined using a Beckman Coulter LS 13320 after dispersion of samples with 0.1 M $Na_4P_2O_7 \cdot 2\ H_2O$ and end-over-end shaking for 12 h. Granulometric characteristics were evaluated using the Gradistatv6 spread sheet (Blott and Pye, 2001). The major- and trace-element compositions were determined on ground samples using X-ray fluorescence (Spectro Xepos) at the Institute of Physical Geography of RWTH Aachen University.

Fourteen samples were taken from archaeological units JVI.1, JVI.2 and JVI.3 for mineralogical analyses at the Laboratory of Geology of the Museo Nacional de Ciencias Naturales of Madrid. One sample from unit JV.3 was taken from the North profile in square I-4. Six samples from unit JVI.2 were taken from the North profile in squares I-4, three from the North profile and one from the East profile in square J8. Two samples from units JVI.1 were taken from the East profile in square J8 and one was taken from the northwest profile in squares F-5/E-5. The mineralogical composition of the mud fraction (<0.063 mm in diameter) was determined by XRD and all samples

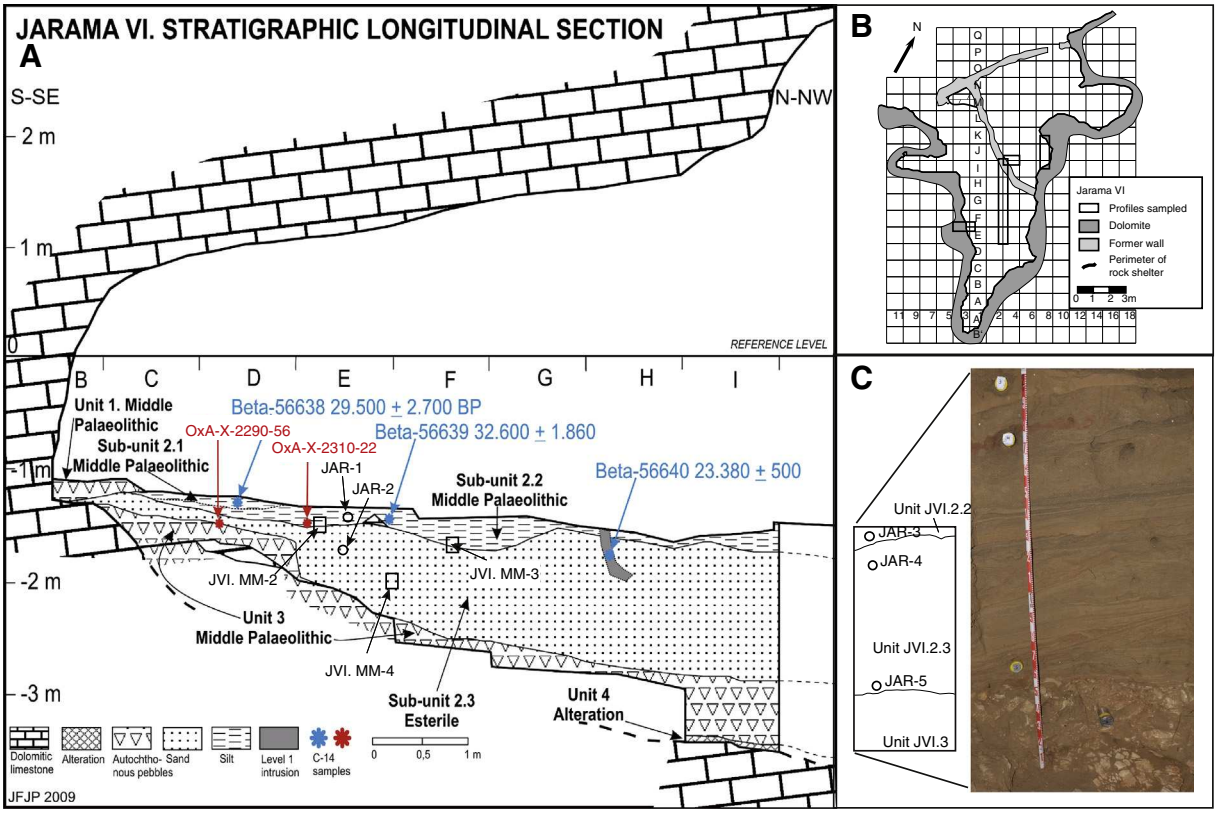

Figure 2. Sketch of West and North profiles (A and C, with orthophoto) with locations of sampling, and excavation map (B).

Please cite this article as: Kehl, M., et al., Late Neanderthals at Jarama VI (central Iberia)?, Quaternary Research (2013), http://dx.doi.org/10.1016/j.yqres.2013.06.010

were analyzed following the dust method for the identification and quantification of the predominant mineral phases (REF?). The analysis was carried out using a Philips PW 1830 X-Ray diffractometer with Cu cathode and a wavelength of Kα = 1.54051, scanning from 3° to 65° 2θ and digital recording Philips PW 1710. The equipment control and the diffractogram profiles studies were managed with the Spanish software XPowder (ver. 2004.04). This program provides a fast qualitative and quantitative identification of samples (Martín-Ramos, 2004).

In order to investigate the microstructure of the deposits, four soil monoliths were extracted from representative parts of units JVI.1, JVI.2.2 and JVI.2.3. The monolith from unit JVI.2.2 includes small red lenses of silty to clayey sediment, which may represent burned soil preserved in the vicinity of the hearth exposed during excavation. All monoliths were impregnated with artificial resin, hardened and cut into 1-cm plates (see Beckmann, 1997 for experimental details). Thin sections, 6 cm wide, 8 cm high and ~30 μm thick, were prepared by Th. Beckmann (Schwülper-Lagesbüttel, Germany). The thin sections were described according to Stoops (2003).

Grain-size distributions, geochemical fingerprints and mineralogy

Considering the whole sediment (coarse and fine fraction), unit JVI.1 is made up of fine gravelly very coarse silty fine sand and corresponds to the textural group of gravelly muddy sands, very poorly sorted, with bimodal grain-size distribution. Subunit JVI.2.1 is composed of very fine sandy very coarse silt included within the textural group of sandy mud, with bimodal distribution and poorly sorted. Subunit JVI.2.2 belongs to the textural group of slightly gravelly sandy mud (slightly very fine gravelly very fine sandy very coarse silt) with unimodal distribution and poorly sorted. Subunit 2.3 belongs to the textural group slightly gravelly muddy sand (slightly medium gravelly very coarse silty fine sand) with unimodal distribution and poorly sorted. Unit JVI.3 is composed of very coarse silty sandy medium gravel and corresponds to the textural group muddy sandy gravel, with bimodal grain-size distribution and very poorly sorted.

Concerning the fine fraction, sand is the dominant grain-size fraction in all samples, whereas silt + clay (mud) amount to a maximum of 43% in sample S9 from unit JVI.1 (Supplementary Table 1). Most samples have unimodal grain-size distributions (Fig. 3) except of samples S1 (unit JVI.2.2) and S9 (unit JVI.1) showing polymodal and sample S3 (unit JVI.2.2) bimodal distributions. The samples S1 and S9 are very poorly sorted showing large D_{10}/D_{90} ratios (Supplementary Table 1). Except of S6 from unit JVI.2.3, all other samples are slightly better sorted. In respect to modal grain size and shape of frequency curves, there is a close similarity of samples S2, S3, S4 (all from unit JVI.2.2) and S7 (from unit JVI.2.3) with comparatively fine grain sizes on the one hand, and the considerably coarser samples S5, S6, S8, S11 (all from unit JVI.2.3) and S10 (from unit JVI.2.1) on the other hand. Most frequency curves are slightly negatively skewed and leptokurtic. The negative skew may be related to elongated mica grains, which, depending on grain orientation during measurement, will be recorded as either sand-sized or silt-sized grains. Sample S11 classifies as pure sand, whereas the other samples belong to the texture class of silty sand. Overall, the granulometric properties of most samples show typical granulometric compositions of fluvial sands and silts, whereas the polymodal grain-size curves of samples S1 and S9 from units JVI.2.2 and JVI.1 suggest a polygenetic origin involving fluvial and gravitational deposits.

The major elements Ca, Mg, S and P indicate distinct differences in the geochemical composition of the samples S1, S9 and S10 taken from unit JVI.2.2, JVI.1 and JVI.2.1 (group 1, Supplementary Table 2), in comparison to the remaining samples which derived from units JVI.2.2 and JVI.2.3 (group 2, Fig. 4). The Ca and Mg contents are highest in samples S1 and S9 and, probably, result from the presence of primary and secondary calcite. Sample S10 (unit JVI.2.1) has a lower Ca and Mg content, but still higher than in most samples from group 2. Sample S6 (unit JVI.2.3), however, shows much higher Ca contents than the other samples of group 2. Sulfur was found in low concentrations in samples of group 1 only. Interestingly, samples from this group also have higher P contents, probably related to accumulation of organic matter. In group 2, the Si and Zr contents show a rather close relationship to the median grain size (m), which is positive between Si and m and negative for Zr and m (Fig. 4B). Sample S11 has the coarsest grain-size distribution and shows the lowest contents of Mg, P, K, Ti, and of most minor elements detected.

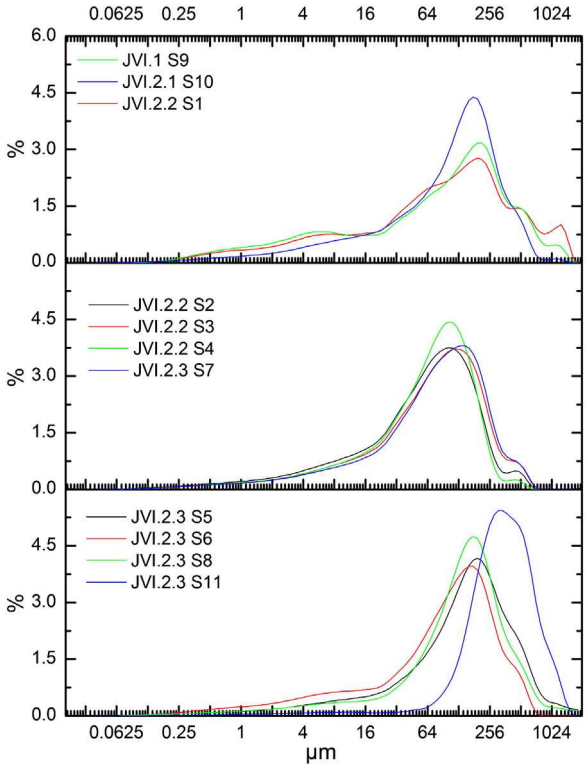

Figure 3. Grain-size distributions of samples S1 to S11.

Overall, the geochemical composition suggests a grouping according to the origin and location of the samples. Those of group 1 are a mixture of allochthonous and autochthonous materials including dolomitic limestone and river-transported shale, quartz and mica. Group 2 encompasses samples from the allochthonous fluvial deposit. The sample S10 takes an intermediate role between the two groups, which also holds for sample S6 in respect to an elevated Ca, content probably related to the presence of secondary calcite.

The mineralogy of the fine fraction of the entire sequence is markedly siliceous with three phases that can be clearly differentiated (Fig. 5; Supplementary Table 3). The lower unit (JVI.3) is characterized by a considerable presence of dolomite (21.8%), accompanied by abundant quartz, feldspars, kaolinite and muscovite/illite. The middle unit (JVI.2) is strongly siliceous with abundant quartz, feldspars, kaolinite and muscovite/illite, with clinochlorite in the reddish silt lense of subunit JVI.2.3. In the upper unit (JVI.1) reappears dolomite (20.6%) accompanied by quartz, muscovite/illite, kaolinite, feldspars and clinochlorite. The mineralogy of the fine fraction of the sediments is comparable with that of the zone and is mainly composed of tectosilicates, phylosilicates and clays originated from the siliceous bedrock (quartzites, shales and schists of the Paleozoic) located upstream from the cavity and transported by the stream of Jarama River. The lower and upper units contain autochthonous-sourced dolomite related with cryoclastic processes.

Please cite this article as: Kehl, M., et al., Late Neanderthals at Jarama VI (central Iberia)?, Quaternary Research (2013), http://dx.doi.org/10.1016/j.yqres.2013.06.010

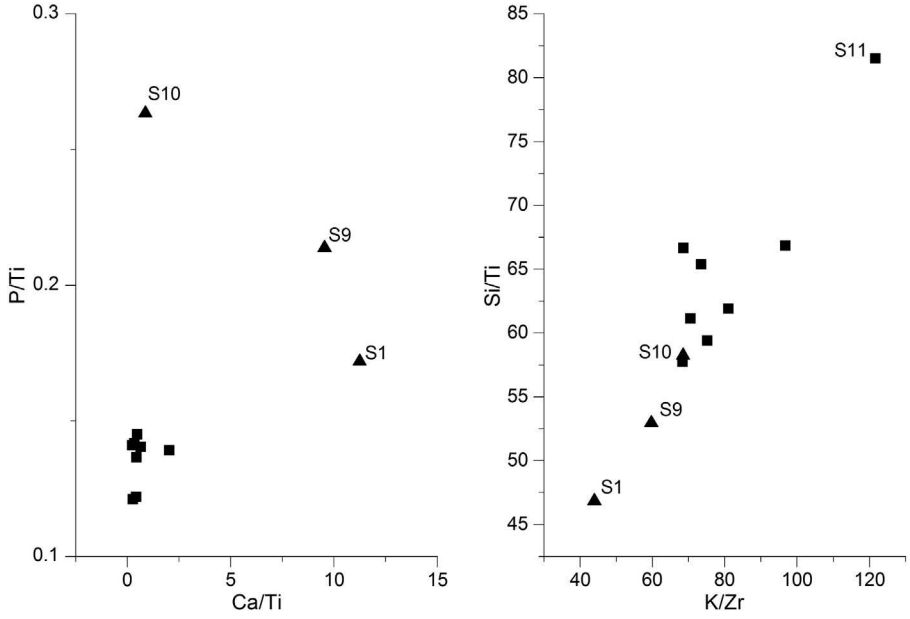

Figure 4. Geochemical fingerprints of cave deposits from units JVI.1 (S1 and S9) and JVI.2.1 (S10) as well as from the fluvial deposits of units JVI.2.2 and JV.2.3 (other samples). The linear relationship between Si/Ti and K/Zr reflects the effect of median grain size, which shows close correlations with Si ($r = 0.610^{**}$, 0.046%, $n = 11$) and Zr ($r = -0.818$, 0.002%, $n = 11$).

Micromorphology

The thin section JAR-M1 from unit JVI.1 shows a poorly sorted mixture of spherical or elongated rock fragments consisting of dolomite, shale and quartzite embedded in a groundmass of and silt grains of quartz, carbonates and very few feldspar and mica (Figs. 6A and B). The dolomite fragments are angular to subangular, while the shale and quartzite fragments show high degree of rounding. In the upper left corner of the section, a strongly fractured limestone fragment is present (Fig. 7A). The longitudinal axes of the elongated shale fragments are often steeply inclined. The porosity is moderately high. Simple packing voids and chitonic to chito-gefuric microstructures are dominant. Locally, abundant vughs are found along with vughy microstructure. Peds are poorly developed. The fine material (<5 μm in diameter) is light yellowish brown and has a dotted appearance reflecting a mixture of fine silt and clay particles. The most prominent pedofeatures are silt cappings and coatings, which cover rock fragments (Figs. 7B and C) and larger mineral grains. The cappings are found on all faces of elongated grains reflecting tilting of the grains after formation of cappings. In some of these coatings, a weakly developed granostriated b-fabric can be observed. Further pedofeatures are rare coatings, incomplete infillings and pendents of micrite.

The thin section shows a detrital sediment containing both frost-shattered dolomite debris from the cave wall and allochtonous

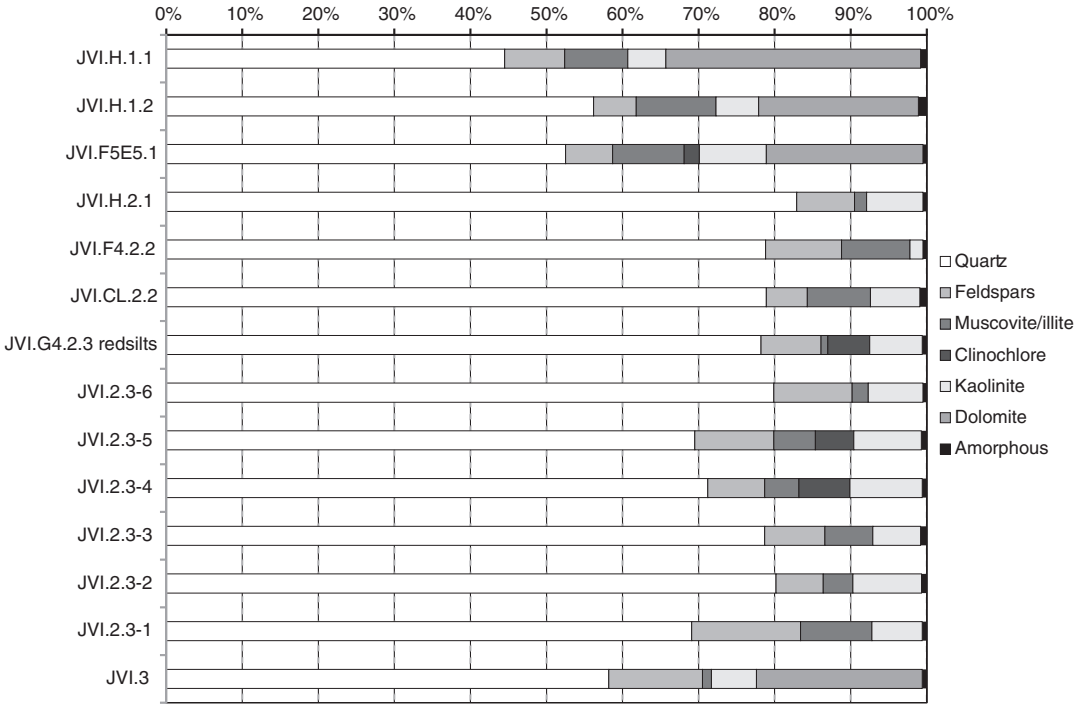

Figure 5. Mineralogical composition of the mud fraction (<0.063 mm).

well-rounded elongated shale fragments, most probably originating from the Jarama River bed. Indications of fluvial accumulation such as bedding, horizontal alignment of elongated grains or lamination are not found. Tilting of elongated grains and occasional silt cappings hint to frequent frost action (cf. Van Vliet Lanoë, 2010) with mixing of the original deposit. Initial development of soil structure and weak carbonate metabolism indicate weak pedogenic alteration of unit JVI.1.

The other thin sections display microlaminated or homogenous well-sorted sands and silty sands mainly consisting of quartz and mica. The long axes of mica grains are often parallel aligned and horizontally to sub-horizontally oriented (Figs. 7D and E). Rock fragments are very rare. The pore space is dominated by simple packing voids and a monic microstructure and c/f related distribution is developed. In thin sections JAR-M3 and JAR-M4 vesicles with a preferred orientation pattern parallel to laminations are common (Figs. 6C and D). These vesicles have probably been formed by entrapped air during rapid deposition of suspended particles.

Reddish-brown lenses of medium silt to clay (Figs. 6C and 7F) are present in thin sections JAR-M 2 and JAR-M 3. The lenses are characterized by compound layering, moderate degree of compaction and frequent shrinkage planes. Locally, microcrusts of sparitic calcite can be found. The clay-rich fine material shows a weakly developed stipple-speckled b-fabric. Fire impact is not apparent. The lenses are interpreted as rip-up clasts of fluvial deposits accumulated under low-energy flow. In thin section JAR-M3 a sharp erosional contact (Fig. 6C) is visible, which delineates the interface between archaeological units JVI.2.2 and 2.3.

Few animal burrows (Figs. 6D and 7G), passage features or root channels are found, indicating limited bioturbation of the fluvial

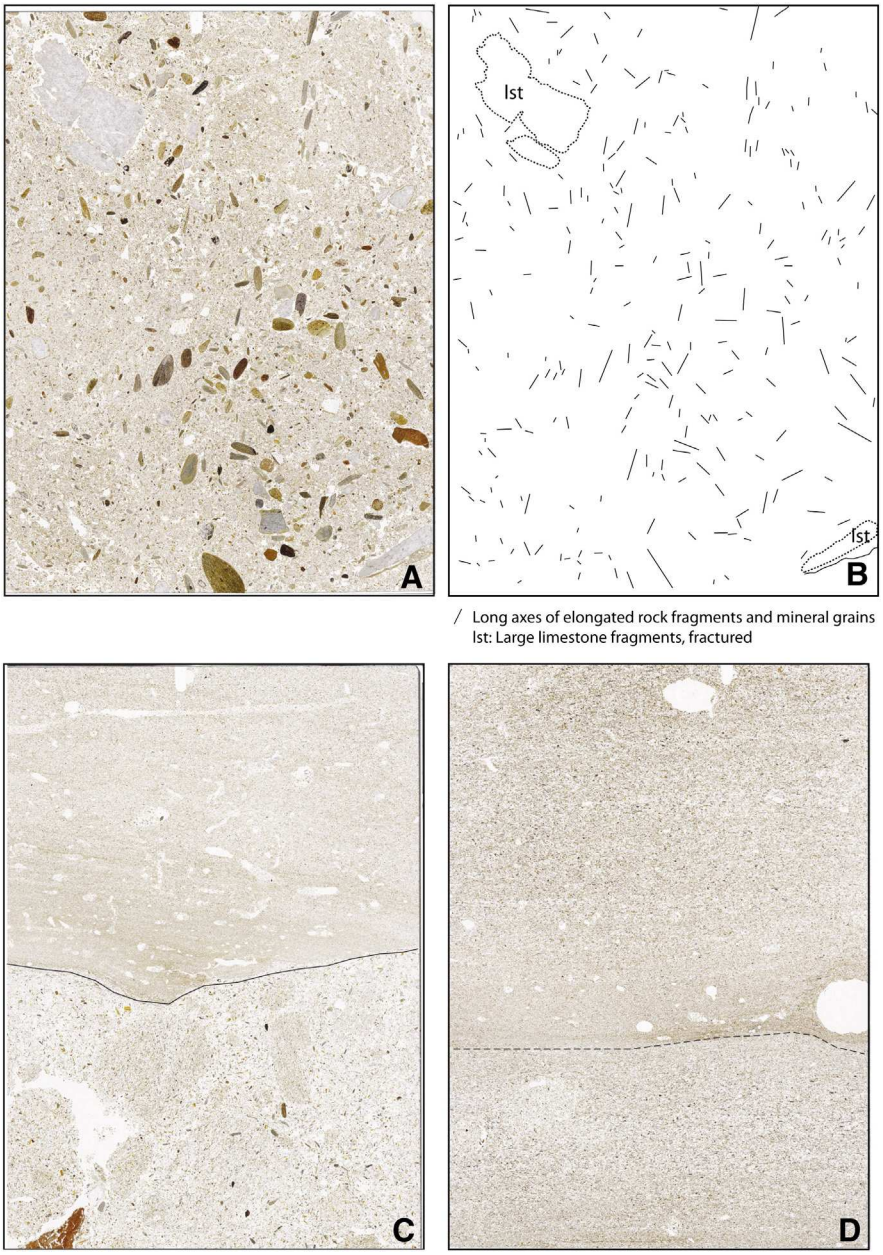

Figure 6. Flatbed scans of thin sections JAR-M1 (A), -M3 (C) and -M4 (D). Note the vertically oriented long axes of grains in A (archaeological unit JVI.1), the brown rip-up clast in the lower left of C and the erosional contact between units JVI.2.2 and JVI.2.3 (solid line in C) as well as the gradual transition between two layers within unit JVI.2.3 (dashed line in D). The original size of the thin sections is 6 cm × 8 cm.

Please cite this article as: Kehl, M., et al., Late Neanderthals at Jarama VI (central Iberia)?, Quaternary Research (2013), http://dx.doi.org/10.1016/j.yqres.2013.06.010

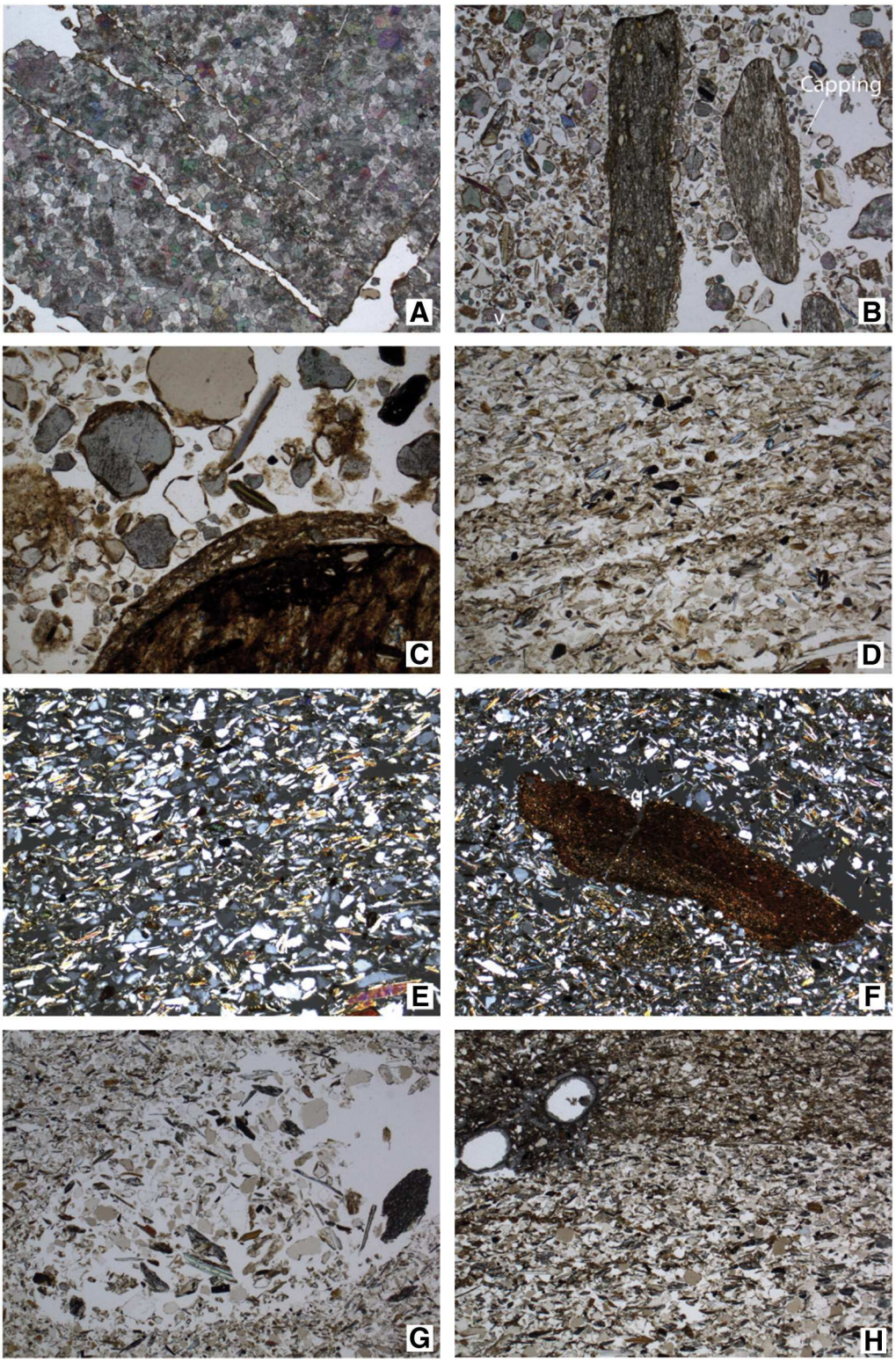

Figure 7. Micrographs from thin sections of Jarama VI. A: Fractured limestone (¿dolomite?) within unit JVI.1 (thin section JAR-M 1, plain polarized light (PPL), frame width is ~5 mm). B: Elongated, well-rounded shale fragments with silt and clay cappings. Note the vertical orientation of the fragments and of the capping (JAR-M 1, PPL, frame width is ~5 mm). C: Silt and clay capping and coatings on rock fragments and mineral grains (JAR-M 1, PPL; frame width ~1.25 mm). D: Silt and clay lenses (unit JVI.2.2) with compound layering in sandy groundmass of JAR-M 2 (partially crossed polarizers (XPLp), pore space is gray, frame width is ~5 mm). These lenses are interpreted as rip-up clasts. E: Banded fabric of groundmass with sub-horizontally aligned elongated mineral grains (JAR-M 2, PPL; frame width ~0.625 mm). F: Same as E, under partially crossed polarizers (XPLp; frame width ~ 0.625 mm). G: Contact between the subunits 4.2 and 4.3 of JAR-M 4. The upper subunit has a finer texture and is more densely packed than the lower one. Note the horizontal orientation of mineral grains in both units. In the upper left two root channels with coatings and hypocoatings of micritic calcite and few calcite infillings are visible (PPL; frame width ~5 mm). H: Animal burrow partially filled with coarse mineral grains and rock fragments (JAR-M 3, PPL, frame width is ~5 mm).

Please cite this article as: Kehl, M., et al., Late Neanderthals at Jarama VI (central Iberia)?, Quaternary Research (2013), http://dx.doi.org/10.1016/j.yqres.2013.06.010

deposits. Instead, the horizontal orientation is often perfectly preserved, also in textural intercalations within macroscopically homogenous sands. Pedofeatures are very rare. Locally, very few calcite coatings and infillings are found, for example at a layer interface within JAR-M4 (Fig. 7H).

Overall, the thin sections from archaeological units JVI.2.2 and 2.3 exhibit well-sorted and commonly microlaminated fluvial sediments with very weak signs of mechanical disturbance and pedogenic alteration.

Radiometric and dosimetric dating

Radiocarbon dating

The results of the three conventional radiocarbon dates (Jordá Pardo, 2001, 2007; Table 1) were described above. The sample locations are projected to the West profile of Figure 2. As reported by Beta Analytic (Florida, USA), each charcoal sample was first boiled/washed free of adhering mineral matter and carefully examined/picked for any intrusive rootlet contamination. The charcoal was then lightly crushed and washed in dilute hot acid and alkali solutions to remove carbonate and humic acid contamination, before being rinsed in hot distilled water, dried, and converted to benzene to enable conventional radiocarbon measurement. The laboratory noted that the carbon content of the samples was low. Not only did this make measurement difficult (the counting time needed to be quadrupled), but also it suggests that the charcoal was poorly preserved and a large proportion of the samples may have been sediment rather than charcoal. Low-carbon charcoals are often found to produce problematic dates, as the sediment component may contain carbon of a different age to the charcoal (Rebollo et al., 2011)

A second series of radiocarbon measurements were conducted on anthropogenically modified bones held in the Universidad de Burgos (Wood et al., in press). Thirty cut-marked bones were selected for %N screening (Brock et al., 2010a, 2012). This technique provides an indication of whether sufficient collagen remains within a bone to enable a radiocarbon date to be produced. Preservation was poor, but using this technique the three bones most likely to contain collagen were selected for dating (JVI.1 (OxA 21714), JVI.2.2 (OxA-X-2310-22) and JVI.3 (OxA-X-2290-56)). The sample locations are projected onto the section drawings in Figure 2 and results of all radiocarbon dates summarized in Table 1.

Radiocarbon dating followed the methods described in Brock et al. (2010b) and Bronk Ramsey et al. (2004). Bones were treated with the ultrafiltration protocol, involving a series of HCl and NaOH washes to remove carbonates and humic acids, gelatinization to take the collagen fraction into solution, filtration with a 60–90 μm Eeze™ filter to remove large insoluble contaminants and ultrafiltration with Vivaspin™ 15 30 kDa MWCO ultrafilter. The purified collagen was combusted in an elemental analyser (e.g., ANCA-GSL) coupled to an isotope ratio-mass spectrometer (e.g., Sercon 20–20) where carbon and nitrogen abundance and stable isotope ratios were measured. The remaining CO_2 was collected cryogenically, converted to graphite over an iron catalyst, and measured in an AMS (Bronk Ramsey et al., 2004). A bone specific pretreatment correction has been subtracted (Wood et al., 2010).

Collagen was extracted from all three bones, but only one (Ox-21714) contained more than the 1% collagen that van Klinken (1999) suggests is required to produce a reliable radiocarbon date. However, all samples had carbon and nitrogen abundances and stable isotope ratios typical of collagen (van Klinken, 1999), suggesting that they are not severely contaminated. Two samples produced radiocarbon dates that are indistinguishable from the laboratory background, and have been ascribed "infinite" dates. The third sample, OxA-X-2310-22, produced a finite date of 49,400 ± 3700 ^{14}C yr BP. Radiocarbon dates become indistinguishable from background when their error exceeds 4000 yr. As this sample is so close to background and has a collagen yield of <1%, it should be regarded as a minimum age estimate and most likely falls beyond the limit of radiocarbon dating.

Luminescence dating

In order to provide a geochronological framework for Jarama VI and to cross-check radiocarbon dating, five samples were extracted from units JVI.2.2 and JVI.2.3 using metal tubes. The samples were dated by luminescence techniques at the laboratory of the Institute of Geography in Cologne. Optically stimulated luminescence (OSL) dates the last exposure of mineral grains to daylight (Huntley et al., 1985). For luminescence dating two parameters have to be determined: the equivalent dose (D_e, Gy), which is the amount of ionizing radiation the sample absorbed during burial, and the dose rate (D_0, Gy ka^{-1}), the amount of energy per unit time released through the decay of naturally occurring radionuclides within and in the surrounding of mineral grains. Several dating protocols are routinely applied on quartz and feldspar to measure the D_e. Partial bleaching of the luminescence signal can result in age overestimation because of insufficiently long or intensive sunlight exposure in fluvial settings, (Olley et al., 1999). Reducing the number of grains simultaneously measured on a sample disk (aliquot; Duller, 2008) or single-grain techniques (Duller et al., 1999; Olley et al., 1999) help to identify fully bleached grains associated with the true depositional age.

Due to their stable signal and better bleachability when compared to feldspar, most studies use quartz for age determination in fluvial settings (Wallinga et al., 2001). However when quartz is not suitable for dating, e.g. the signal is saturated, ages can still be obtained by infrared stimulated luminescence (IRSL) on feldspar, if present in the sample. Potassium-rich feldspars have the advantages of bright luminescence signals and a higher saturation dose allowing for extending the potential dating range. However the optical signal of feldspar is reported to be less light sensitive, i.e. it is harder to bleach (e.g., Godfrey-Smith et al., 1988; Lowick et al., 2012). The greatest disadvantage of feldspar is a phenomenon referred to as anomalous fading (Wintle, 1973), which is thought to be the result of quantum mechanical tunneling (Visocekas, 1979) that leads to a loss of signal over time. In order to overcome a resulting age underestimation, several approaches have been proposed to correct for the observed fading (e.g., Huntley and Lamothe, 2001; Kars et al., 2008) or by measuring elevated temperature feldspar signals, which are less prone to fading (Buylaert et al., 2009, 2012; Thiel et al., 2011).

All preparation procedures for the determination of the equivalent dose were carried out under subdued red illumination, following standard procedures (Wintle, 1997). By sieving and chemical treatment the purified quartz and K-rich feldspars in the grain-size range of 100–150 μm were extracted for dating. Estimation of the external dose rate was conducted using a high-resolution gamma-ray spectrometer with a high purity germanium detector. The cosmic ray dose rates were calculated according to Prescott and Hutton (1994), taking into consideration the altitude and geomagnetic latitude of the sampling site and the thickness, density and water content of the overlying sediments. Additionally the attenuation of cosmic-rays in the overlying rock was accounted for and a correction for the geometric shielding by the rock shelter was incorporated using the equations given by Dunne et al. (1999). Measured present-day water contents varied between 0.3 and 2.0% (Supplementary Table 4). These values probably underestimate the annual mean water content because sampling was conducted after the hot and dry summer season. Considering the weak intensity of weathering of the sediment, it is, however, not likely that water contents had been much higher in the past. We therefore estimated a mean annual water content of 5.0%. All dose rate data are summarized in Supplementary Table 4.

Please cite this article as: Kehl, M., et al., Late Neanderthals at Jarama VI (central Iberia)?, Quaternary Research (2013), http://dx.doi.org/10.1016/j.yqres.2013.06.010

Measurements of the equivalent dose followed standard single-aliquot regenerative-dose (SAR) procedures for quartz (Murray and Wintle, 2000, 2003; Wintle and Murray, 2006) and feldspar (Wallinga et al., 2000). Considering the depositional context of the sediments this protocol was first applied to quartz due to its better signal bleachability. However, quartz signals were found to be in or close to saturation for all samples (i.e., $>2 \cdot D_0$, Wintle and Murray, 2006; Supplementary Fig. 1), probably because of the high average environmental dose rate of 3.8 Gy ka^{-1}. Thus no quartz OSL ages could be obtained. Therefore the infrared stimulated luminescence (IRSL) of potassium-rich feldspars was measured, which saturates at higher doses compared to quartz. In addition, we adopted modified elevated temperature post-IR IRSL (pIRIR) protocols from Buylaert et al. (2009; $pIRIR_{225}$) and Thiel et al. (2011; $pIRIR_{290}$) (Supplementary Table 5) to minimize a probable signal underestimation induced by fading.

The bleachability of both pIRIR signals was tested by measuring residual doses after increasing exposure time to UV light in a Hönle SOL2 solar simulator and sunlight. In both cases the $pIRIR_{225}$ signal yielded lower residual doses and thus bleaches faster than the $pIRIR_{290}$ signal (Supplementary Fig. 2). The applicability of the pIRIR protocols to the samples investigated in this study was further tested by dose recovery tests. While the $pIRIR_{225}$ protocol was able to successfully recover the given laboratory dose of 374 Gy (measured/given dose ratio 0.98 ± 0.02 and 0.99 ± 0.02), the $pIRIR_{290}$ protocol could not recover the given dose within 10% from unity (1.25 ± 0.27 and 1.20 ± 0.04) (Supplementary Fig. 3).

Considering the results of bleaching and dose recovery tests, the $pIRIR_{225}$ protocol was found to be the more appropriate approach for D_e measurements of the samples under study here. Between 14 and 16 individual equivalent doses were determined for each of the five samples. Despite the $pIRIR_{290}$ protocol not being able to successfully recover a laboratory dose and its higher residual doses, 11 individual equivalent doses were determined for sample JAR-3 using this protocol. This was done in order to validate the assumption that there will be a considerable difference in D_e and hence in calculated ages between $pIRIR_{290}$ and $pIRIR_{225}$ protocols. The relative spread in equivalent doses after taking measurement uncertainties into account, termed overdispersion (OD), varies between 8 and 10% for all samples except JAR-3. The latter has higher OD values of 17% and 13% for the $pIRIR_{225}$ and $pIRIR_{290}$ protocol, respectively. Additionally, for sample JAR-2 and JAR-3 equivalent doses were determined using the conventional $IRSL_{50}$ dating protocol measuring the feldspar signal at 50 °C. As expected due to a likely occurrence of fading, the obtained equivalent doses were considerably lower than those obtained by $pIRIR_{225}$ or $pIRIR_{290}$. In order to correct for the loss of signal over time, fading tests were conducted. Mean *g*-values of 3.0 ± 0.9 (JAR-2, n = 11) and 3.9 ± 0.9 (JAR-3, n = 11) were calculated using the equations given by Huntley and Lamothe (2001). No fading corrections were applied to pIRIR signals, as measured fading rates of these signals have been argued as potential laboratory artifacts (Thomsen et al., 2008; Buylaert et al., 2009, 2012; Thiel et al., 2011).

Equivalent doses for age calculation were determined using the central age model (Galbraith et al., 1999) and the age model after Fuchs and Lang (2001) for the $pIRIR_{225}$ D_e distribution of sample JAR-3. For a complete summary of results on equivalent dose and dose rate determination see Table 3. The calculated luminescence ages for all samples and protocols are shown in Figure 8 and expanded upon in the Discussion section below.

Re-evaluation of the archaeological sequence

As mentioned previously, the Jarama VI lithic assemblage has been tentatively attributed to the Middle Paleolithic (units JV.2 and JV.3), and Early Upper Paleolithic (unit JVI.1) (Jordá Pardo, 2001). A recent study and reassessment of this material, summarized below, concludes that all three units show technological characteristics that may be attributed to the Middle Paleolithic.

Raw material

The raw material acquisition strategy is nearly identical on all three levels. Quartz is the most frequently used material, followed by quartzite, both of autochthonous origin. Their possible source areas have been located in the immediate environs of the site.

The case of flint is different. It composes just 7% of the assemblage, in contrast to quartz (62%), and has a minority presence on all levels (9% on unit JVI.1; 4% on unit JVI.2 and 7% on unit JVI.3). Its exact origin is still unknown, but it is definitely allochthonous as there is no naturally occurring flint within 10 km of the site. Other materials such as rock crystal, slate, dolomite and others complete the spectrum.

The studied assemblage consists of 1833 items, 323 of which are from unit JVI.1, 342 from unit JVI.2 and 1168 from unit JVI.3. These totals do not include fragments. A remarkably large percentage of cobbles was found on all three levels (see Table). Detailed analysis of these cobbles has found very few with percussion marks or evidence of having been part of the lithic tool production sequence. They were almost certainly brought into the cave by men, given that there is no other possible explanation for their presence at this site.

Unit JVI.1

Forty-seven of the 323 analyzed items from unit JVI.1 were quartz, quartzite and fibrolite. Twenty-two of them (5 quartzite, 2 fibrolite and 15 quartz), were used for percussion.

The cores include 31 quartz and one quartzite item. Eight of the quartz cores are fractured, while the others include eleven bifacials, eleven unifacials, and multifacials. The most frequent system is centripetal, followed by items with orthogonal negatives and unifacials. The quartzite core is centripetal bifacial. These items generally have a cortex on one face, and initial or moderate exploitation (none are exhausted). One was tested and discarded due to its poor material quality, and another (Carbonell et al., 1999) shows evidence of heavy recurrent unifacial work. The lithic reduction system on unit JVI.1 can be described as non-specific and opportunistic.

Among the 220 blank flakes, 65% are quartz, 21% quartzite, 9% flint and 5% rock crystal. Most butts are non-cortical, platform and unifaceted, and 32% are cortical with non-faceted butts. 20% of the dorsal surfaces have a cortex. Several flakes are débordante, in some cases Levallois. Some flakes are from discoidal exploitation systems, and three flint flakes are burnt.

Seven of the 24 formal tools are fractured. They have similar technical characteristics to the flakes, the majority unifaceted with a non-cortical platform and non-cortical dorsal surfaces. With unifacial retouches and a generally simple angle, the types include ten denticulates, seven notches, a side scraper, a double-side scraper (Fig. 9, 1), an end scraper (Fig. 9, 2), three flakes with simple retouch and a partially retouched item (Fig. 9, 3).

The lithic production system as well as the collection of tools contradicts the attribution to an Early Upper Paleolithic as proposed by Jordá Pardo (2001). The lithic assemblage for JVI.1 reflects a clear Middle Paleolithic association, as does the lower two units JVI.2 and JVI.3.

Unit JVI.2

An assemblage of 343 items was recovered on the upper levels of this unit, including 179 cobbles, of which 24 quartz and quartzite items bear percussion marks and evidence of use. Twenty-one of the cores are quartz and quartzite, and one is flint.

The 21 cores discovered in unit JVI.2 give a clear picture of the applied lithic reduction system. As in unit JVI.1 mostly unspecific and opportunistic reduced flake cores are dominant (17 cores). Only

Please cite this article as: Kehl, M., et al., Late Neanderthals at Jarama VI (central Iberia)?, Quaternary Research (2013), http://dx.doi.org/10.1016/j.yqres.2013.06.010

Table 3
Dose rate data, equivalent doses and IRSL ages for five samples from Jarama VI.

Unit	Laboratory CODE	Sample	Mineral[a]	Protocol	Number of aliquots accepted/measured[b]	Age model[c]	Overdispersion OD (%)[d]	Equivalent dose D_e (Gy)[e,f]	Cosmic ray dose rate (Gy ka^{-1})[g]	Total dose rate D_0 (Gy ka^{-1})[h]	$g_{2\ days}$ (%/decade)	Luminescence age (ka)[i]
JVI.2.2	C-L3140	JAR-1	FS	$pIRIR_{225}$	16/16	CAM	8.0 ± 0.5	243 ± 13	0.089 ± 0.018	4.63 ± 0.50	–	52.5 ± 4.9
JVI.2.2	C-L3004	JAR-3	FS	$pIRIR_{225}$	15/16	F/L	16.5 ± 1.3	250 ± 24	0.097 ± 0.019	4.45 ± 0.64	–	58.8 ± 6.8
				$pIRIR_{290}$	11/11	CAM	13.0 ± 1.1	371 ± 25	0.097 ± 0.019	4.25 ± 0.49	–	87.4 ± 8.2
				$IRSL_{50}$	16/16	CAM	9.1 ± 0.5	165 ± 9	0.097 ± 0.019	3.05 ± 0.43	3.9 ± 0.9	*38.8 ± 3.3*
												53.9.7 ± 6.9
JVI.2.3	C-L3141	JAR-2	FS	$pIRIR_{225}$	15/15	CAM	9.8 ± 0.6	215 ± 12	0.080 ± 0.016	4.06 ± 0.46	–	53.0 ± 5.2
				$IRSL_{50}$	15/15	CAM	7.2 ± 0.4	150 ± 8	0.080 ± 0.016	3.21 ± 0.46	3.0 ± 0.9	*36.9 ± 3.5*
												46.6 ± 5.9
JVI.2.3	C-L3005	JAR-4	FS	$pIRIR_{225}$	14/14	CAM	9.7 ± 0.6	196 ± 11	0.090 ± 0.018	3.35 ± 0.34	–	58.6 ± 5.1
JVI.2.3	C-L3006	JAR-5	FS	$pIRIR_{225}$	14/14	CAM	10.2 ± 0.7	226 ± 13	0.060 ± 0.012	3.94. ± 0.41	–	57.2 ± 4.9

[a] FS = feldspar. For all samples the 100–150 μm grain-size fraction was used.
[b] Aliquots were rejected if a) the test dose signal was less than three times the instrumental background, b) the recycling ratio of signals induced by duplicate regenerative doses was less than 0.9 or above 1.1 (Murray and Wintle, 2000), c) the recuperation rate was greater than 5% of the natural signal (Aitken and Smith 1988), and d) the sensitivity-corrected natural signal was above $2 \cdot D_o$, so that no reliable D_e estimate could be obtained.
[c] CAM = central age model, F/L = model after Fuchs and Lang (2001).
[d] The overdispersion was calculated using the central age model.
[e] For all samples and protocols, recycling ratios are within 10% of unity (1.02 ± 0.03 in average) and recuperation rates remained below 3% of the natural signal.
[f] For the $pIRIR_{225}$ and $pIRIR_{290}$ protocol residual doses of 2.79 Gy and 18.11 Gy respectively were subtracted from the equivalent dose used for age calculation.
[g] The cosmic ray dose rate was calculated using the equations given by Prescott and Hutton (1994), with additional consideration of cosmic ray attenuation in the rock shelter roof and a correction for the configuration of the cave (Dunne et al., 1999). To account for any uncertainties associated with cosmic dose rate calculation an error of 20% was implemented.
[h] When calculating the total dose rate a long term average water content of 5 ± 3% was assumed for all samples. For feldspar samples an a-value of 0.07 ± 0.02 (Preusser et al., 2005) was used to account for external α-dose rate and a K concentration of 12.5 ± 0.5% (Huntley and Baril, 1997) was assumed.
[i] Luminescence ages in italics are non fading-corrected $IRSL_{50}$ ages.

3 cores prove the existence of a surface-oriented conception, which corresponds with the Levallois recurrent centripetal method (Fig. 10, 14–16). The realization of the applied method is very simple and makes use mostly of given configurations of the used pebbles: natural surfaces on the lower surface and crude preparation of the striking platform or simple secondary use of negatives from lower-surface preparation.

The majority (77%) of the 119 flakes are quartz. Almost 50% have cortical and non-cortical butts, which can also be seen on the dorsal surfaces and the cores, suggesting that the blanks were not prepared prior to their exploitation.

The butt surfaces are platform in 90% of cases, and almost 50% are unifaceted. We have detected siret fractures, discoidal flakes, a few Kombawa, many debordante and plunging flakes. The quartzite items are slightly larger than the quartz, although all have micro and small formats (Bagolini). The two chert flakes are Levallois.

There are eleven formal tools in quartz, one in quartzite, ten in chert and a single one in rock crystal. The sample comprising 22 formal tools is composed of nine side scrapers (Fig. 10, 4–11), three convergent side scrapers (Fig. 10, 1–3), one notched piece (Fig. 10, 12), one burin (Fig. 10, 13), one bec, three denticulates, two points (including one pseudo-Levallois point), one quartz notched on blade and one retouched flake. Together, they reflect a typical late Middle Paleolithic association. Some of the formal tools in chert are on Levallois flakes and one is burnt.

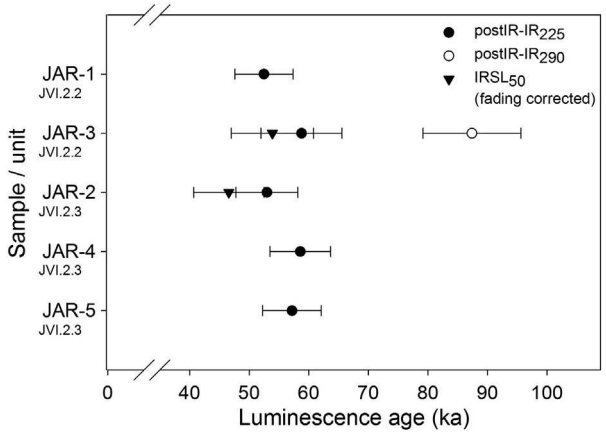

Figure 8. Summary of IRSL ages for all samples, and for all protocols. Residual doses were subtracted (Table 3) and a systematic error of 5% associated with the beta source calibration was taken into account before age calculation. The error bars represent 1-sigma errors.

Unit JVI.3

The lowest archaeological unit has yielded the richest collection. We have retrieved 1168 lithic tools, including 178 cobbles in different materials, of which scarcely 30 were used.

Under the lithic remains, 95 cores and 21 formal tools were detected. In contrast to the upper levels the lithic production system in unit JVI.3 is quite diverse. Beside the omnipresent unspecific and opportunistic reduced flake cores (63), the discoidal method with (6) and without flat base (5) and different methods following the surface conception—Levallois preferential unidirectional (2), Levallois recurrent unidirectional (4) and centripetal (14)—are present (Fig. 11, 22–24; Fig. 11, 25–26; Fig. 12, 4–5; Fig. 12, 1–3; Fig. 11, 16–21). Additionally a single core was reduced corresponding to the Le Pucheuil-type method (Fig. 12, 6). It is important to note that natural pebble surfaces as well as flake lower surfaces are integrated in every core reduction strategy, either Levallois or not. This underlines the economic use of local pebbles and the integration of given convexities in the construction of the cores.

There are 810 flakes, many of which are from discoidal cores. 25% of the butts are from cortical flakes, primarily platform and uni- and bi-faceted, and 82% of the dorsal surfaces are non-cortical. No cortical butts have been found among the flint flakes. More of this material was used than in the case of quartz or quartzite, suggesting that the blanks were prepared prior to their exploitation.

As with unit JVI.2, denticulated quartz flakes and chert side scrapers predominate the assemblage of 84 formal tools, which include several types of side scraper (Fig. 11, 1–7), including lateral and convergent side scrapers (Fig. 11, 11–15), and three double side scraper (Fig. 11, 8–10).

Discussion

New radiometric dating of the site, new stratigraphic data and the re-evaluation of the lithic inventory shed new light on human

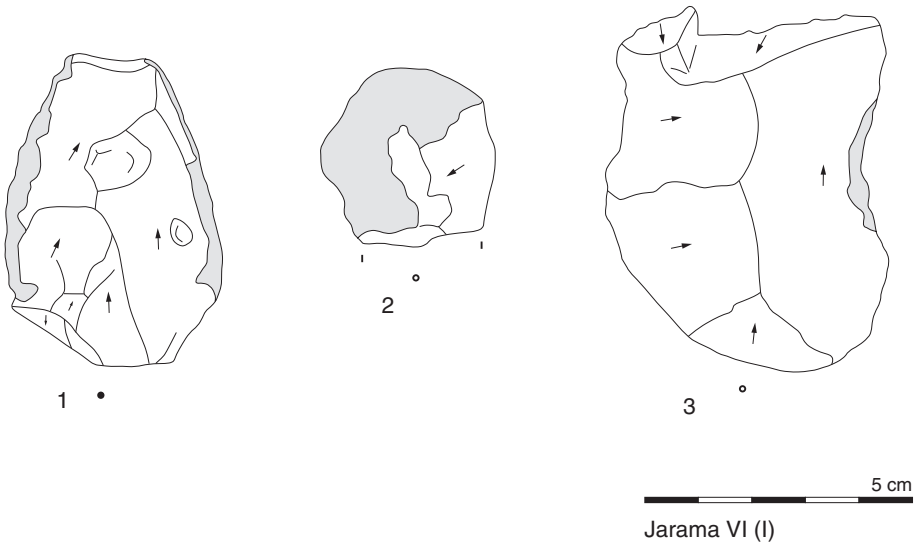

Figure 9. Unit JVI.1: Formal tools on flakes: double side scraper (1), end scraper (2), and partial retouched piece (3) (gray shading = retouch).

occupation of Jarama VI (central Iberia) and provide important information on the purported late survival of Neanderthals in the region.

Processes of sediment accumulation and alteration

The accumulation of rock shelter deposits at Jarama VI took place in five main depositional phases. During a first phase, fragments of the dolomite roof were deposited simultaneously to human occupation; during the second phase, these autochthonous fragments located in the external part of the rock shelter were reworked and mixed with sands and gravel of the Jarama River. A rich artifact assemblage indicates intensive use of the cave by Neanderthals (unit JVI.3).

The third phase during accumulation of units J.VI.2.3 to 2.1 started with partial erosion of the underlying sediments followed by deposition of fluvial fines with very low gravitational input of dolomitic limestone blocks from the cave wall. The granulometric composition and cuneiform sediment package suggest that fluvial accumulation occurred during exceptional high flood events, when runoff spilled

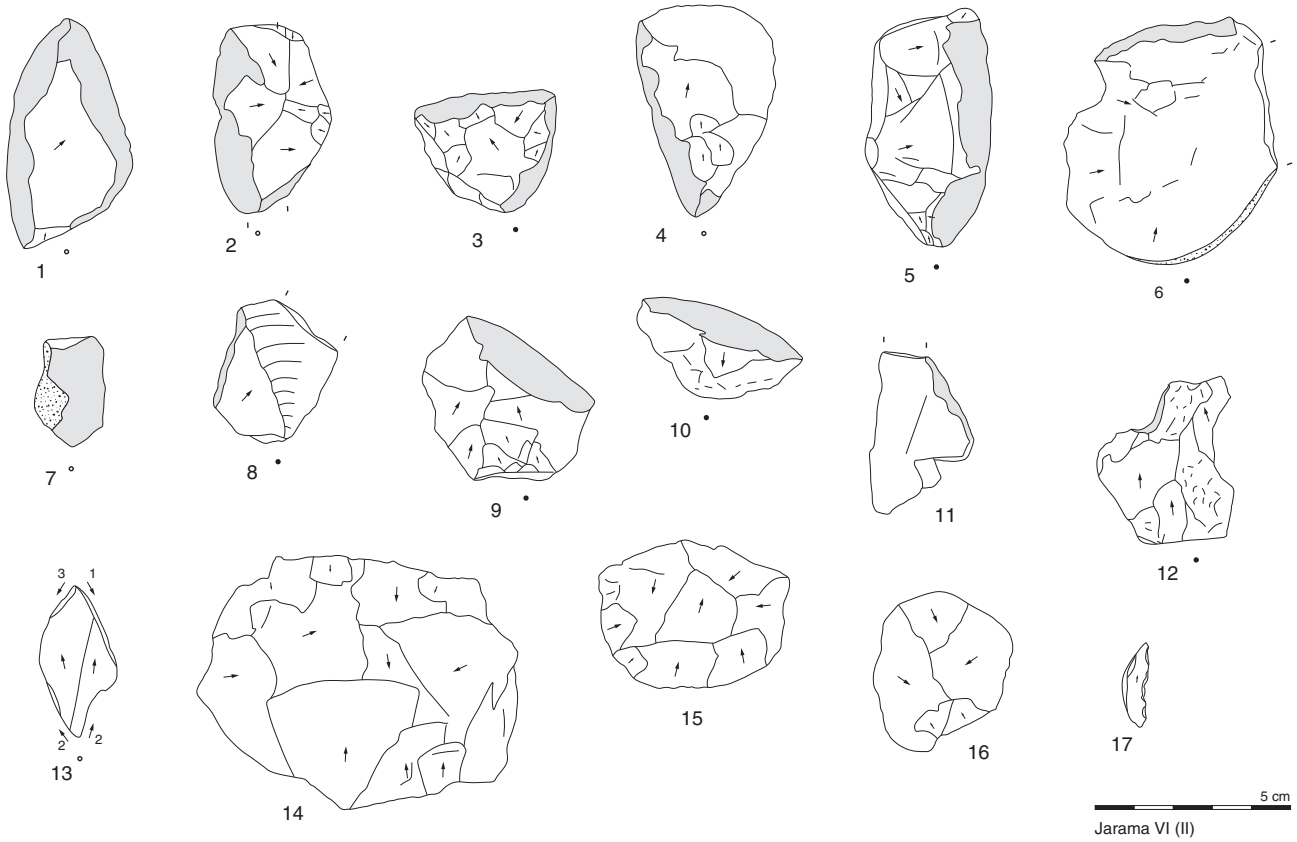

Figure 10. Unit JVI.2: Formal tools on flakes: convergent side scraper (1–3), side scraper (4–11), notched piece (12) and burin (13). Core configuration: recurrent centripetal (surface conception) (14–16) and unretouched bladelet (17). The unretouched bladelet (17) is documented to prevent a confusion in classification because the object looks like a Châtelperron point (gray shading = retouch).

Please cite this article as: Kehl, M., et al., Late Neanderthals at Jarama VI (central Iberia)?, Quaternary Research (2013), http://dx.doi.org/10.1016/j.yqres.2013.06.010

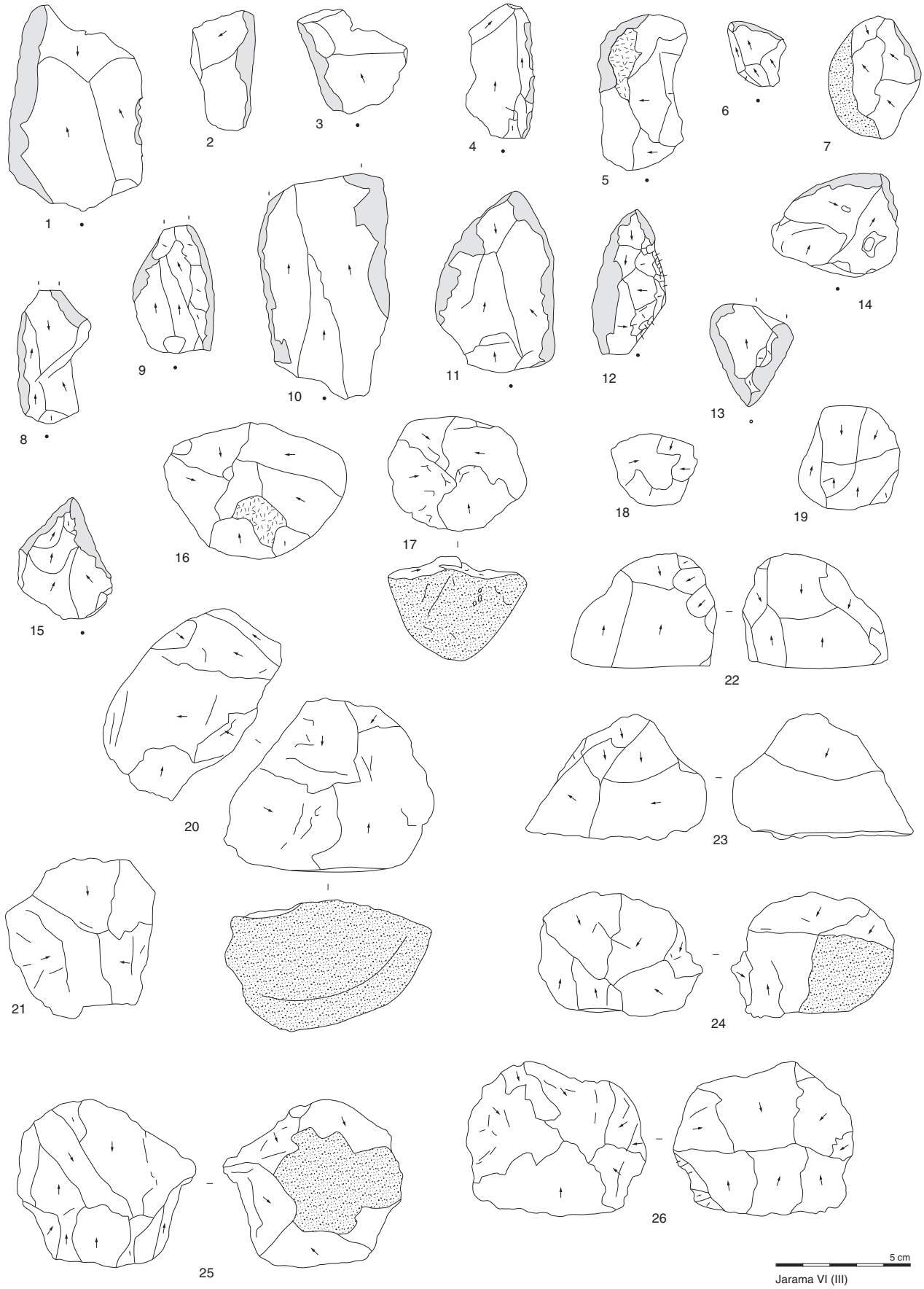

Figure 11. Unit JVI.3: Formal tools on flake: side scraper (1–7), double-side scraper (8–10), convergent side scraper (11–15). Core configuration — recurrent centripetal (surface conception) (16–21), bifacial (volume conception) (22–24) and recurrent centripetal (volume conception) (25–26) (gray shading = retouch).

Please cite this article as: Kehl, M., et al., Late Neanderthals at Jarama VI (central Iberia)?, Quaternary Research (2013), http://dx.doi.org/10.1016/j.yqres.2013.06.010

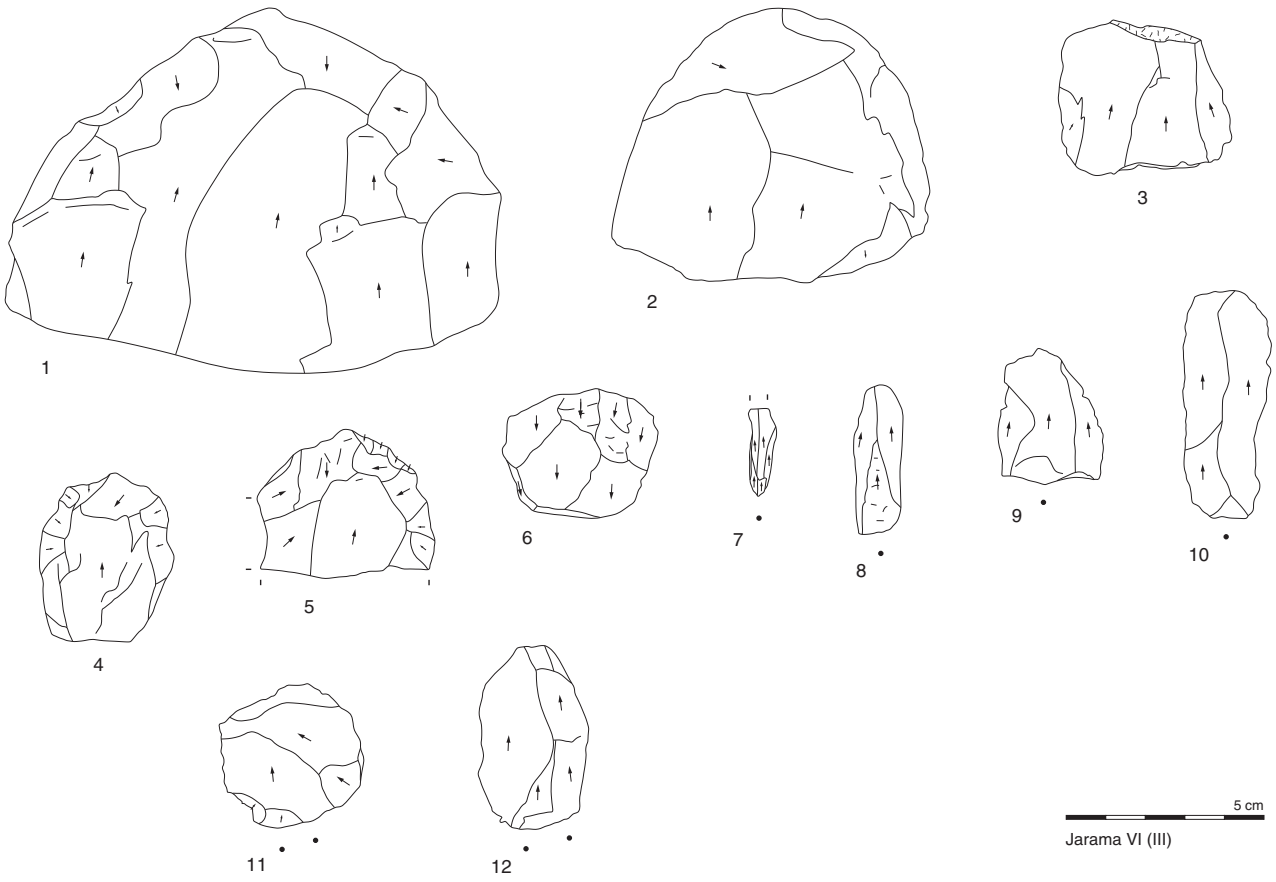

Figure 12. Unit JVI.3: Core configuration: recurrent unidirectional (surface conception) (1–3), preferential unidirectional (surface conception) (4–5), and Le Pucheuil-type unidirectional (volume conception) (6).

over the bedrock sill at the entrance of the cave. Entering the rock shelter, runoff velocity decreased leading to deposition of comparatively fine sediments ranging from silty very fine sands to medium sands. The sediments are preserved, since they were probably protected from later floods by the bedrock sill or blocks collapsed near the cave entrance. The sediment properties and the hydraulic and geomorphological conditions suggest that unit JVI.2 consists of slackwater flood deposits, which typically accumulate well above the mean water table at protected niches of the valley slopes or of gorges and canyons during exceptional floods (e.g., Thorndycraft and Benito, 2006; Woodward et al., 2001). These deposits are also reported from the catchments of Jarama and Tagus rivers (Alonso and Garzón, 1996; Benito et al., 2003). Radiometric dating of slackwater deposits in Central Spain, however, has focused on Holocene sequences so far (cf. Thorndycraft and Benito, 2006).

Near the entrance of the rock shelter, several phases of deposition and erosion were identified in unit VI 2.3. The comparatively sharp erosional contacts between units JVI.2.3 and 2.2 and the occasional occupancy by humans during accumulation of JVI.2.2 and 2.1 suggest that deposition occurred during several high flood events. The preservation of the hearth feature in JVI.2.2 indicates comparatively low energy of flow in the interior part of the cave. The duration of sedimentary hiatuses in between depositional periods is difficult to assess. We expect that hiatuses were short, because homogenization and mechanical disturbance of sediment layers by bioturbation and pedogenic alteration are very limited. Also, pedogenic alteration and weathering of the sediments is very weak.

The contact between unit JVI.1 and JVI.2 is well marked by the lithological difference between the two units. The contact consists of a paraconformity and represents a short stratigraphical diastema that preceded the onset of the fourth depositional phase. Unit JVI.1 is composed of a mixture of autochthonous and allochthonous sediments: common dolomite spall originates from the cave wall, whereas fine gravel and sands were emplaced by low-energy processes like sheetwash. On the upper surface of JVI.2, marks or impressions left by well-rounded allochthonous pebbles and cobbles are detected. Those coarse components were probably brought into the shelter by humans during the sedimentation of unit JVI.1 (Jordá Pardo, 2007). Frost features are common, indicating that the sediment was more strongly affected by moisture and temperature changes than the underlying deposits. These changes contributed to increased intensity of weathering and pedogenic alteration.

The last depositional phase yielded chemical precipitates of the stalagmitic crust in unit JVI.0, which sealed the sequence in the interior part of the cave. It cemented angular dolomite debris from the cave wall, accumulated on the surface of unit JVI.1 over an unknown period of time.

Chronological framework

Recent re-dating of sites on the Iberian Peninsula has put into question the reliability of young radiocarbon dates from Middle Paleolithic context (e.g., Zilhão et al., 2011) and the prolonged survival of Neanderthals (Wood et al., in press). Recent improvements in the pretreatment of radiocarbon samples (Bird et al., 1999; Higham, 2011) mean Neanderthal occupations dated with the routine ABA protocol often increase in age when redated using new techniques such as ABOx-SC of charcoal or ultrafiltration of bone collagen (Higham, 2011). Given the new dates from Jarama VI on collagen extracted with an ultrafiltration protocol, the previous radiocarbon dates on charcoal pretreated with an ABA protocol (Beta-56639, Beta-56638 and Beta-56640) must be rejected. The

Please cite this article as: Kehl, M., et al., Late Neanderthals at Jarama VI (central Iberia)?, Quaternary Research (2013), http://dx.doi.org/10.1016/j.yqres.2013.06.010

new ultrafiltration dates suggest that the entire sequence is likely to fall beyond the limit of the radiocarbon method at ca. 50 ^{14}C ka BP.

Samples taken from unit JVI.2.2 were dated to 52.5 ± 4.9 ka (JAR-1, C-L3140) and 58.8 ± 6.8 ka (JAR-3, C-L3004) by the pIRIR$_{225}$ protocol. The observed overdispersion in D_e values of JAR-3 (C-L3004; Supplementary Table 4) being perceptibly larger than in all other samples and the D_e distribution indicate poor re-setting of the IRSL signals during transport. Post-depositional mixing of sediments causing the spread in D_es can be ruled out as there is no clear sedimentological evidence. For JAR-3 (C-L3004) the application of the model of Fuchs and Lang (2001) seems to be a reliable method to identify fully bleached grains associated with the true depositional age. This assumption is supported by the fact that both JAR-1 (C-L3140) and JAR-3 (C-L3004) are from the same stratigraphic unit and hence should yield comparable age estimates. Further evidence is provided by the fading-corrected IRSL$_{50}$ age of 53.9 ± 6.9 ka for JAR-3 (C-L3004), which is in good agreement with both the pIRIR$_{225}$-ages of the same sample and JAR-1 (C-L3140). The pIRIR$_{290}$-age of 87.4 ± 8.2 ka for JAR-3 (C-L3004) is most likely overestimated, since the pIRIR$_{290}$ signal suffers from large residual doses (Supplementary Fig. 2) and the protocol is not able to successfully recover an artificial laboratory dose (Supplementary Fig. 3). Samples taken from unit JVI.2.3 yielded pIRIR$_{225}$-ages of 53.0 ± 5.2 ka (JAR-2, C-L3141), 58.6 ± 5.1 ka (JAR-4, C-L3005) and 57.2 ± 4.9 ka (JAR-5, C-L3006). The fading-corrected IRSL$_{50}$ age of 46.6 ± 5.9 ka for sample JAR-2 (C-L3141) seems to underestimate the true depositional age. However a homogeneity test (see Galbraith, 2003; Galbraith and Roberts, 2012) provides evidence that all age estimates of unit JVI.2.3 are consistent ($P = 0.42$) with a common value. We therefore propose a weighted mean pIRIR$_{225}$-age of 56.3 ± 2.9 ka for unit JVI.2.3 ($P = 0.73$).

The new radiocarbon and luminescence age estimates suggest that the whole sequence is older than previously thought (Jordá Pardo, 2001, 2007).

Cultural attribution

Consistent differences in the way the raw material was handled have been found on all three levels: tiny and exhausted cores, products without cortex and retouched flakes with resharpening edges in the case of flint. Quartzite and quartz were not used in the same way, as the cores seem to have been left in an initial state of exploitation, without prior reduction, due to the local availability of this raw material and flakes and formal tools with cortex on butts and dorsal surfaces. It should be noted that the quantitative difference between the assemblages on the three levels is due to the different size of the areas dug on each one, although the intensity of visits to the caves may not have been constant.

The present technological analysis confirms the observation that the lithic assemblages found on the three levels at Jarama VI correspond to the Middle Paleolithic. The exploitation systems and the types of products, both retouched and non-retouched, along with the standard Neanderthal morphotypes (denticulates and sidescrapers on flakes) all correspond to this period.

Expeditive strategies of flake production and denticulate, notch and scraper configuration have been found on units JVI.1 and JVI.2, while unit JVI.3 contains more elaborated production sequences, although the former characteristics are also present.

During the late Pleistocene, Neanderthal groups may have inhabited several caves and open air sites in the Jarama Valley, which in the case of the Jarama VI rock shelter clearly seem to be a technological continuum that ended in the first half of MIS 3. After the abandonment of the site by Neanderthals no reoccupation in the late Pleistocene is evident. Scattered surface finds from later prehistoric context indicate ephemeral occupation events only. This setting supports the idea of a chronological hiatus between the last Neanderthals and the first modern humans in central Iberia (Schmidt et al., 2012).

Conclusions

New granulometric, mineralogic and micromorphological data corroborate the previous hypothesis that the central part of the sequence at Jarama VI (unit JVI.2) accumulated as slackwater deposits during several superfloods. In contrast to this unit of allochthonous sediments, units JVI.3 and JVI.1 contain larger amounts of autochthonous dolomite and manuports from outside the cave.

The cultural sequence and chronological framework of Jarama VI needed to be revised. The lithic inventory of unit JVI.1, previously attributed to the Early Upper Paleolithic, has a clear Mousterian affinity; hence the cave does not record the transition from Middle to Upper Paleolithic in central Iberia. New radiocarbon and luminescence dating of the sequence shows that the main occupation at Jarama VI documented in units JVI.2 and JVI.3 ended before about 50 ka. Jarama VI does not provide evidence for a late survival of Neanderthals in central Iberia. However, due to its rich archaeological material Jarama VI is a key site in the area for the study of the Middle Paleolithic. In addition, the fluvial sequence of the site provides highly interesting objects for the study of slackwater deposits in the Jarama River valley.

Supplementary data to this article can be found online at http://dx.doi.org/10.1016/j.yqres.2013.06.010.

Acknowledgments

This study was carried out under the project “Prehistoric Research on the Upper Jarama Valley (Valdesotos, Guadalajara, Spain)” authorized by the Autonomous Government of Castilla-La Mancha (Spain) and directed by J.F. Jordá Pardo. Laboratory work by Mariane Dohms (Physical Geography of RWTH Aachen University) and Rafael Martínez (MNCN, Madrid) and fruitful discussions of laboratory results with Jens Protze (Physical Geography of RWTH Aachen University) are gratefully acknowledged. We are grateful for the financial support by the C1 project of the CRC 806 “Our way to Europe,” funded by the German Research Foundation (DFG). One of us (A.P.) also received support from the DFG research project “Der Übergang vom Mittel-zum Jungpaläolithikum in Südwesteuropa. Modelluntersuchungen zur Steingerätetechnologie” (WE 1022/8).

References

Adán Alvarez, G., Arribas Herrera, A., Barbadillo, J., Cervera García, J., Estrada García, R., García Valero, M.A., Jordá Pardo, J.F., Pastor Muñoz, J., Sánchez Chillón, B., Sánchez Marco, A., Sanchiz, B., Sesé, C., 1995. Prospecciones y excavaciones arqueológicas en el Alto Valle del Jarama (Valdesotos, Guadalajara, Castilla-La Mancha). In: Balbín, R., de Valiente, J., Musat, M.T. (Eds.), Arqueología en Guadalajara. Patrimonio Histórico - Arqueología Castilla - La Mancha, 12. Junta de Comunidades de Castilla La Mancha, Toledo, pp. 111–124.

Alonso, A., Garzón, G., 1996. The Jarama River. In: Benito, G., Pérez-González, A., Machado, M.J., de Alba, S. (Eds.), Palaeohydrology in Spain: Field Excursion Guide. Second International Meeting on Global Continenal Palaeohydrology, GLOCOPH '96, pp. 21–34.

Atlas Climático Ibérico, sine ano. Temperatura del aire y precipitación (1971–2000). Agencia Estatal de Meteorología de España and Departamento de Meteorologia e Clima, Instituto de Meteorologia de Portugal.79 pp.

Beckmann, Th., 1997. Präparation bodenkundlicher Dünnschliffe für mikromorphologische Untersuchungen. Hohenheimer Bodenkundliche Hefte 40, 89–103.

Benito, G., Sánchez-Moya, Y., Sopeña, A., 2003. Sedimentology of high-stage flood deposits of the Tagus River, Central Spain. Sedimentary Geology 157, 107–132.

Bicho, N., Carvalho, A.F., González-Sainz, C., Sanchidrián, J.L., Villaverde, V., Straus, L.G., 2007. The Upper Paleolithic Rock Art of Iberia. Journal of Archaeological Method and Theory 14, 81–151.

Bird, M.I., Ayliffe, L.K., Fifield, L.K., Turney, C.S.M., Cresswell, R.G., Barrows, T.T., David, B., 1999. Radiocarbon dating of “old” charcoal using a wet oxidation, stepped-combustion procedure. Radiocarbon 41, 127–140.

Blott, S.J., Pye, K., 2001. Gradistat: a grain size distribution and statistics package for the analysis of unconsolidated sediments. Earth Surface Processes and Landforms 26, 1237–1248.

Brock, F., Higham, T., Ramsey, C.B., 2010a. Pre-screening techniques for identification of samples suitable for radiocarbon dating of poorly preserved bones. Journal of Archaeological Science 37, 855–865.

Brock, F., Higham, T., Ditchfield, P., Ramsey, C.B., 2010b. Current pretreatment methods for AMS radiocarbon dating at the Oxford Radiocarbon Accelerator Unit (ORAU). Radiocarbon 52, 103–112.

Brock, F., Wood, R., Higham, T.F.G., Ditchfield, P., Bayliss, A., Bronk Ramsey, C., 2012. The reliability of nitrogen content (%N) as an indicator of collagen preservation suitable for radiocarbon dating. Radiocarbon 54, 879–886.

Bronk Ramsey, C., 2009. Bayesian analysis of radiocarbon dates. Radiocarbon 51, 337–360.

Bronk Ramsey, C.B., Higham, T.F.G., Leach, P., 2004. Towards high-precision AMS: progress and limitations. Radiocarbon 46, 17–24.

Buylaert, J.P., Murray, A.S., Thomsen, K.J., Jain, M., 2009. Testing the potential of an elevated temperature IRSL signal from K-feldspar. Radiation Measurements 44, 560–565.

Buylaert, J.P., Jain, M., Murray, A.S., Thomsen, K.J., Thiel, C., Sohbati, R., 2012. A robust feldspar luminescence dating method for Middle and Late Pleistocene sediments. Boreas 41, 435–451.

Cacho, C., Martos, J.A., Jordá, J., Yravedra, J., Avezuela, B., Valdivia, J., Martín, I., 2010. El Paleolítico superior en el interior de la Península Ibérica. Revisión crítica y perspectivas de futuro. El Paleolítico superior peninsular, Novedades del, siglo XXI. 115–136.

Carbonell, E., Márquez, B., Mosquera, M., Ollé, A., Rodríguez, X.P., Sala, R., Vergés, J.Mª., 1999. El Modo 2 en Galería. Análisis de la industria lítica y sus procesos técnicos. Atapuerca: Ocupaciones humanas y paleoecología del yacimiento de Galería. Arqueología de Castilla y León, 7, pp. 299–352 (Memorias).

Delibes de Castro, G., Díez Martín, F., 2006. ¿Una Meseta desolada? Estado actual de la investigación sobre el Paleolítico Superior en las regiones interiores de la Península Ibérica. In: Delibes de Castro, En G., Díez Martín, F. (Eds.), El Paleolítico Superior en la Meseta Norte española. Studia Archaeologica, 94. Universidad de Valladolid, Fundación Duques de Soria, Valladolid, pp. 11–40.

Díez, C., García, M.A., Gil, E., Jordá Pardo, J.F., Ortega, A.I., Sánchez, B., Sánchez, A., 1988–89. La Cueva de Valdegoba (Burgos). Primera campaña de excavaciones. Zephyrvs XLI-XLII, 56–74.

Díez, C., Alonso, R., Bengoechea, A., Colina, A., Jordá, J.F., Navazo, M., Ortiz, J.E., Pérez, S., Torres, T., 2008. El paleolítico medio en el valle del Arlanza (Burgos). Los sitios de la Ermita, Millán y la Mina. Revista Cuaternario y Geomorfología 22, 135–157.

Duller, G.A.T., 2008. Single-grain optical dating of Quaternary sediments: why aliquot size matters in luminescence dating. Boreas 37, 589–612.

Duller, G.A.T., Bøtter-Jensen, L., Murray, A.S., Truscott, A.J., 1999. Single grain laser luminescence (SGLL) measurements using a novel automated reader. Nuclear Instruments and Methods in Physics Research B 155, 506–514.

Dunne, J., Elmore, D., Muzikar, P., 1999. Scaling factors for the rates of production of cosmogenic nuclides for geometric shielding and attenuation at depth on sloped surfaces. Geomorphology 27, 3–11.

Finlayson, C., Carrión, J.S., 2007. Rapid ecological turnover and its impact on Neanderthal and other human populations. Trends in Ecology & Evolution 22, 213–222.

Finlayson, C., Giles Pacheco, F., Rodríguez-Vidal, J., Fa, D.A., Gutierrez López, J.M., Santiago Pérez, A., Finlayson, G., Allueé, E., Baena Preysler, J., Cáceres, I., Carrión, J.S., Fernández Jalvo, Y., Gleed-Owen, C.P., Jimenez Espejo, F., López, P., López Sáez, J.A., Riquelme Cantal, J.A., Sánchez Marco, A., Giles Guzman, F., Brown, K., Fuentes, N., Valarino, C.A., Villalpando, A., Stringer, C.B., Martinez Ruiz, F., Sakamoto, T., 2006. Late survival of Neanderthals at the southernmost extreme of Europe. Nature 443, 850–853.

Fuchs, M., Lang, A., 2001. OSL dating of coarse-grain fluvial quartz using single-aliquot protocols on sediments from NE Peloponnese, Greece. Quaternary Science Reviews 20, 783–787.

Galbraith, R.F., 2003. A simple homogeneity test for estimates of dose obtained using OSL. Ancient TL 21, 75–77.

Galbraith, R.F., Roberts, 2012. Statistical aspects of equivalent dose and error calculation and display of OSL dating: an overview and some recommendations. Quaternary Geochronology 11, 1–27.

Galbraith, R.F., Roberts, R.G., Laslett, G.M., Yoshida, H., Olley, J.M., 1999. Optical dating of single and multiple grains of Quartz from Jinmium rock shelter, northern Australia: part I, experimental design and statistical models. Archaeometry 41, 339–364.

Godfrey-Smith, D.L., Huntley, D.J., Chen, W.H., 1988. Optically dating studies of quartz and feldspar sediment extracts. Quaternary Science Reviews 7, 373–380.

González-Sampériz, P., Leroy, S.A.G., Carrión, J.S., Fernández, S., García-Antón, M., Gil-García, M.J., Uzquiano, P., Valero-Garcés, B., Figueiral, I., 2010. Steppes, savannahs, forests and phytodiversity reservoirs during the Pleistocene in the Iberian Peninsula. Review of Palaeobotany and Palynology 162, 427–457.

Higham, T., 2011. European Middle and Upper Palaeolithic radiocarbon dates are often older than they look: problems with previous dates and some remedies. Antiquity 85, 235–249.

Higham, T., Brock, F., Peresani, M., Broglio, A., Wood, R., Douka, K., 2009. Problems with radiocarbon dating the Middle to Upper Palaeolithic transition in Italy. Quaternary Science Reviews 28, 1257–1267.

Higham, T., Basell, L., Jacobi, L., Wood, R., Bronk Ramsey, C., Conard, N.J., 2012. Testing models for the beginnings of the Aurignacian and the advent of figurative art and music: the radiocarbon chronology of Geisenklosterle. Journal of Human Evolution 62, 664–676.

Hublin, J.-J., Barroso, C., Medina, P., Fontugne, M., Reyss, J.-L., 1995. The Mousterian Site of Zafarraya (Andalucia, Spain): dating and implications on the paleolithic peopling processes of Western Europe. Comptes-Rendus de l'Académie des Sciences de Paris. 321, 931–937.

Huntley, D.J., Lamothe, M., 2001. Ubiquity of anomalous fading in K-feldspars and the measurement and correction for it in optical dating. Canadian Journal of Earth Sciences 38, 1093–1106.

Huntley, D.J., Godfrey-Smith, D.I., Thewalt, M.L.W., 1985. Optical dating of sediments. Nature 313, 105–107.

ITGE 1990. Mapa Geológico de España. Escala 1:50.000. 485 (20–19) Valdepeñas de la Sierra. Instituto Tecnológico Geominero de España, Madrid.

Jennings, R., Finlayson, C., Fa, D., Finlayson, G., 2011. Southern Iberia as a refuge for the last Neanderthal populations. Journal of Biogeography 38, 1873–1885.

Jordá Pardo, J.F., 1993. El poblamiento prehistórico en el sector sur-oriental del Sistema Central peninsular (Alto Valle del Jarama, Guadalajara, España). Trabalhos de Antropologia e Etnologia 33, 99–117.

Jordá Pardo, J.F., 2001. Dataciones isotópicas del yacimiento del Pleistoceno Superior de Jarama VI (alto valle del jarama, Guadalajara, España) y sus implicaciones cronoestratigráficas. In: Büchner, D. (Ed.), Studien *in memoriam* Wilhelm Schüle. Rahden/Westfalen, pp. 225–235.

Jordá Pardo, J.F., 2007. The wild river and the last Neanderthals: a palaeoflood in the geoarchaeological record of the Jarama Canyon (Central Range, Guadalajara province, Spain). Geodinamica Acta 20, 209–217.

Kars, R.H., Wallinga, J., Cohen, K.M., 2008. A new approach towards anomalous fading correction for feldspar IRSL dating — tests on samples in field saturation. Radiation Measurements 43, 786–790.

Lorenzo, C., Navazo, M., Díez, J.C., Sesé, C., Arceredillo, D., Jordá Pardo, J.F., 2012. New human fossil to the last Neanderthals in central Spain (Jarama VI, Valdesotos, Guadalajara, Spain). Journal of Human Evolution 62 (6), 720–725.

Lowick, S.E., Trauerstein, M., Preusser, F., 2012. Testing the application of post IR-IRSL dating to fine grain waterlain sediments. Quaternary Geochronology 8, 33–40.

Maroto, J., Vaquero, M., Arrizabalaga, Á., Baena, J., Baquedano, E., Jordá, J., Julià, R., Montes, R., van der Plicht, J., Rasines, P., Wood, R., 2012. Current issues in late Middle Palaeolithic chronology: New assessments from Northern Iberia: the Neanderthal home: spatial and social behaviours. Quaternary International 247, 15–25.

Martín-Ramos, J.D., 2004. Xpowder. A software package for powder x-ray diffraction analysis. (www.xpowder.com).

Moreno, A., González-Sampériz, P., Morellón, M., Valero-Garcés, B.L., Fletcher, W.J., 2012. Northern Iberian abrupt climate change dynamics during the last glacial cycle: a view from lacustrine sediments. Quaternary Science Reviews 36, 139–153.

Moure, J.A., García-Soto, Y.E., 2000. Economie et utilisation du territoire pendant le Moustérien de la vallée moyenne de l'Arlanza (Burgos, Espagne). Anthropologie et Préhistoire 11, 186–189.

Muñoz Muñoz, J., Aldeanueva, R.A., Rey Arnaiz, J.M., 1989. El clima de la provincial de Guadalajara. Paralelo 37, 227–251.

Murray, A.S., Wintle, A.G., 2000. Luminescence dating of quartz using an improved single-aliquot regenerative-dose protocol. Radiation Measurements 32, 57–73.

Murray, A.S., Wintle, A.G., 2003. The single aliquot regenerative dose protocol: potential for improvements in reliability. Radiation Measurements 37, 377–381.

Navazo, M., Diéz, J.C., 2008. Prado Vargas y la variabilidad tecnológica a finales del Paleolítico medio en la Meseta norte. Treballs d'Arqueología 14, 121–139.

Olley, J.M., Caitcheon, G.G., Roberts, R.G., 1999. The origin of dose distributions in fluvial sediments, and the prospect of dating single grains from fluvial deposits using optically stimulated luminescence. Radiation Measurements 30, 207–217.

Ortiz, J.E., Moreno, L., Torres, T., Vegas, J., Ruiz-Zapata, B., García-Cortés, Á., Galán, L., Pérez-González, A., 2013. A 220 ka palaeoenvironmental reconstruction of the Fuentillejo maar lake record (Central Spain) using biomarker analysis. Organic Geochemistry 55, 85–97.

Prescott, J.R., Hutton, J.T., 1994. Cosmic ray contributions to dose rates for luminescence and ESR dating: large depths and long-term time variations. Radiation Measurements 23, 497–500.

Rebollo, N.R., Weiner, S., Brock, F., Meignen, L., Goldberg, P., Belfer-Cohen, A., Bar-Yosef, O., Boaretto, E., 2011. New radiocarbon dating of the transition from the Middle to the Upper Paleolithic in Kebara Cave, Israel. Journal of Archaeological Science 38, 2424–2433.

Reimer, P.J., Baillie, M.G.L., Bard, E., Bayliss, A., Beck, J.W., Blackwell, P.G., Bronk Ramsey, C., Buck, C.E., Burr, G.S., Edwards, R.L., Friedrich, M., Grootes, P.M., Guilderson, T.P., Hajdas, I., Heaton, T.J., Hogg, A.G., Hughen, K.A., Kaiser, K.A., Kromer, B., Mccormac, F.G., Manning, S.W., Reimer, R.W., Richards, D.A., Southon, J.R., Talamo, S., Turney, C.S.M., Van Der Plicht, J., Weyhenmeyer, C.E., 2009. IntCal09 and Marine09 radiocarbon age calibration curves, 0–50,000 years cal BP. Radiocarbon 59, 1111–1150.

Schmidt, I., Bradtmöller, M., Kehl, M., Pastoors, A., Tafelmaier, Y., Weninger, B., Weniger, G.-C., 2012. Rapid climate change and variability of settlement patterns in Iberia during the Late Pleistocene: temporal and spatial corridors of *Homo sapiens sapiens* population dynamics during the Late Pleistocene and Early Holocene. Quaternary International 274, 179–204.

Thiel, C., Buylaert, J.P., Murray, A., Terhorst, B., Hofer, I., Tsukamoto, S., Frechen, M., 2011. Luminescence dating of the Stratzing loess profile (Austria): testing the potential of an elevated temperature post-IR IRSL protocol. Quaternary International 234, 23–31.

Thomsen, K.J., Murray, A.S., Jain, M., Bøtter-Jensen, L., 2008. Laboratory fading rates of various luminescence signals from feldspar-rich sediment extracts. Radiation Measurements 43, 1474–1486.

Thorndycraft, V.R., Benito, G., 2006. Late Holocene fluvial chronology of Spain: the role of climatic variability and human impact. Catena 66, 34–41.

Van Klinken, G.J., 1999. Bone collagen quality indicators for palaeodietary and radiocarbon measurements. Journal of Archaeological Science 26, 687–695.

Van Vliet Lanoë, B., 2010. Frost Action. In: Stoops, G., Marcelino, V., Mess, F. (Eds.), Interpretation of Micromorphological Features of Soils and Regoliths. Elsevier, Amsterdam, pp. 81–108.

Vegas, J., Ruiz-Zapata, B., Ortiz, J.E., Galán, L., Torres, T., García-Cortés, Á., Gil-García, M.J., Pérez-González, A., Gallardo-Millán, J.L., 2010. Identification of arid phases during the last 50 cal. ka BP from the Fuentillejo maar-lacustrine record (Campo de Calatrava Volcanic Field, Spain). Journal of Quaternary Sciences 25, 1051–1062.

Please cite this article as: Kehl, M., et al., Late Neanderthals at Jarama VI (central Iberia)?, Quaternary Research (2013), http://dx.doi.org/10.1016/j.yqres.2013.06.010

Visocekas, R., 1979. Miscellanous aspects of artificial TL of calcite: emission spectra athermal detrapping and anomalous fading. PACT 3, 258–265.
Wallinga, J., Murray, A.S., Wintle, A.G., 2000. The single-aliquot regenerative-dose (SAR) protocol applied to coarse-grain feldspar. Radiation Measurements 32, 529–533.
Wallinga, J., Murray, A.S., Duller, G.A.T., Törnqvist, T.E., 2001. Testing optically stimulated luminescence dating of sand-sized quartz and feldspar from fluvial deposits. Earth and Planetary Science Letters 193, 617–630.
Wintle, A.G., 1973. Anomalous fading of thermoluminescence in mineral samples. Nature 245, 143–144.
Wintle, A.G., 1997. Luminescence dating: laboratory procedures and protocols. Radiation Measurements 27, 769–817.
Wintle, A.G., Murray, A.S., 2006. A review of quartz optically stimulated luminescence characteristics and their relevance in single-aliquot regeneration dating protocols. Radiation Measurements 41, 369–391.
Wood, R.E., Higham, T.F.G., Bronk Ramsey, C., 2010. Refining background corrections for radiocarbon dating of bone collagen at ORAU. Radiocarbon 52, 600–611.
Wood, R.E., Barroso, C., Caparros, M., Jorda, J.F., Galvan Santos, B., Higham, T.F.G., 2013. Radiocarbon dating casts doubt on the late chronology of the Middle to Upper Palaeolithic transition in southern Iberia. Proceedings of the National Academy of Sciences 110, 2781–2786 (in press).
Woodward, J., Hamlin, R., Macklin, M., Karkanas, P., Kotjabopoulou, E., 2001. Quantitative sourcing of slackwater deposits at Boila rockshelter: a record of lateglacial flooding and Paleolithic settlement in the Pindus Mountains, Northwest Greece. Geoarchaeology 16, 501–536.
Zilhão, J., 2006. Chronostratigraphy of the Middle-to-upper Paleolithic transition in the Iberian peninsula. Pyrenae 37, 7–84.
Zilhão, J., Cardoso, J.L., Pike, A.W.G., Weninger, B., 2011. Gruta Nova da Columbeira (Bombarral, Portugal): Site stratigraphy, age of the Mousterian sequence, and implications for the timing of Neandertal extinction in Iberia. Quartär 58, 93–112.

Please cite this article as: Kehl, M., et al., Late Neanderthals at Jarama VI (central Iberia)?, Quaternary Research (2013), http://dx.doi.org/10.1016/j.yqres.2013.06.010